

5-2-2013

# Synthesis and biological evaluation of novel folic acid receptor-targeted, $\beta$ -cyclodextrin-based drug complexes for cancer treatment

Juan-Juan Yin  
*University of South Florida*

Sonali Sharma  
*University of South Florida*

Stepan P. Shumyak  
*University of South Florida*

Zhi-Xin Wang  
*University of South Florida*

Zhi-Wei Zhou  
*University of South Florida*

*See next page for additional authors*

**Right click to open a feedback form in a new tab to let us know how this document benefits you.**

Follow this and additional works at: [https://uknowledge.uky.edu/nanobio\\_facpub](https://uknowledge.uky.edu/nanobio_facpub)

 Part of the [Pharmacy and Pharmaceutical Sciences Commons](#)

## Repository Citation

Yin, Juan-Juan; Sharma, Sonali; Shumyak, Stepan P.; Wang, Zhi-Xin; Zhou, Zhi-Wei; Zhang, Yangde; Guo, Peixuan; Li, Chen-Zhong; Kanwar, Jagat R.; Yang, Tianxin; Mohapatra, Shyam S.; Liu, Wanqing; Duan, Wei; Wang, Jian-Cheng; Li, Qi; Zhang, Xueji; Tan, Jun; Jia, Lee; Liang, Jun; Wei, Ming Q.; Li, Xiaotian; and Zhou, Shu-Feng, "Synthesis and biological evaluation of novel folic acid receptor-targeted,  $\beta$ -cyclodextrin-based drug complexes for cancer treatment" (2013). *Nanobiotechnology Center Faculty Publications*. 1.  
[https://uknowledge.uky.edu/nanobio\\_facpub/1](https://uknowledge.uky.edu/nanobio_facpub/1)

---

**Authors**

Juan-Juan Yin, Sonali Sharma, Stepan P. Shumyak, Zhi-Xin Wang, Zhi-Wei Zhou, Yangde Zhang, Peixuan Guo, Chen-Zhong Li, Jagat R. Kanwar, Tianxin Yang, Shyam S. Mohapatra, Wanqing Liu, Wei Duan, Jian-Cheng Wang, Qi Li, Xueji Zhang, Jun Tan, Lee Jia, Jun Liang, Ming Q. Wei, Xiaotian Li, and Shu-Feng Zhou

**Synthesis and biological evaluation of novel folic acid receptor-targeted,  $\beta$ -cyclodextrin-based drug complexes for cancer treatment****Notes/Citation Information**

Published in *PLoS ONE*, v. 8, no. 5, e62289.

© 2013 Yin et al. This is an open-access article distributed under the terms of the Creative Commons Attribution License, which permits unrestricted use, distribution, and reproduction in any medium, provided the original author and source are credited.

**Digital Object Identifier (DOI)**

<http://dx.doi.org/10.1371/journal.pone.0062289>

# Synthesis and Biological Evaluation of Novel Folic Acid Receptor-Targeted, $\beta$ -Cyclodextrin-Based Drug Complexes for Cancer Treatment

Juan-Juan Yin<sup>1</sup>, Sonali Sharma<sup>1</sup>, Stepan P. Shumyak<sup>1</sup>, Zhi-Xin Wang<sup>1</sup>, Zhi-Wei Zhou<sup>1</sup>, Yangde Zhang<sup>2</sup>, Peixuan Guo<sup>3</sup>, Chen-Zhong Li<sup>4</sup>, Jagat R. Kanwar<sup>5</sup>, Tianxin Yang<sup>6</sup>, Shyam S. Mohapatra<sup>7</sup>, Wanqing Liu<sup>8</sup>, Wei Duan<sup>9</sup>, Jian-Cheng Wang<sup>10</sup>, Qi Li<sup>11</sup>, Xueji Zhang<sup>12</sup>, Jun Tan<sup>13,14,15</sup>, Lee Jia<sup>16</sup>, Jun Liang<sup>1</sup>, Ming Q. Wei<sup>17</sup>, Xiaotian Li<sup>18</sup>, Shu-Feng Zhou<sup>1\*</sup>

**1** Department of Pharmaceutical Sciences, College of Pharmacy, University of South Florida, Tampa, Florida, United States of America, **2** National Hepatobiliary and Enteric Surgery Research Center, Xiangya Hospital, Central South University, Changsha, Hunan, China, **3** Nanobiotechnology Center and Markey Cancer Center, College of Pharmacy, University of Kentucky, Lexington, Kentucky, United States of America, **4** Nanobioengineering and Bioelectronics Laboratory, Department of Biomedical Engineering, Florida International University, Miami, Florida, United States of America, **5** Nanomedicine-Laboratory of Immunology and Molecular Biomedical Research (LIMBR), Centre for Biotechnology and Interdisciplinary Biosciences and Institute for Frontier Materials (IFM), Deakin University, Waurn Ponds, Victoria, Australia, **6** Department of Internal Medicine, University of Utah and Salt Lake Veterans Affairs Medical Center, Salt Lake City, Utah, United States of America, **7** Nanomedicine Research Center and Division of Translational Medicine, Department of Internal Medicine, Morsani College of Medicine, University of South Florida, Tampa, Florida, United States of America, **8** Department of Medicinal Chemistry and Molecular Pharmacology, College of Pharmacy, Purdue University, West Lafayette, Indiana, United States of America, **9** School of Medicine, Deakin University, Waurn Ponds, Victoria, Australia, **10** State Key Laboratory of Natural and Biomimetic Drugs, School of Pharmaceutical Science, Peking University, Beijing, China, **11** Department of Oncology, Shuguang Hospital (Western Campus), Shanghai University of Traditional Chinese Medicine, Shanghai, China, **12** Research Center for Bioengineering and Sensing Technology, University of Science and Technology Beijing, Beijing, China, **13** James A. Haley Veterans' Administration Hospital, Tampa, Florida, United States of America, **14** Department of Neurosurgery and Brain Repair, Center of Excellence for Aging and Brain Repair, Morsani College of Medicine, University of South Florida, Tampa, Florida, United States of America, **15** Department of Psychiatry and Behavioral Neurosciences, Silver Child Development Center, Rashid Laboratory for Developmental Neurobiology, Morsani College of Medicine, University of South Florida, Tampa, Florida, United States of America, **16** Cancer Metastasis Alert and Prevention Center, College of Chemistry and Chemical Engineering, Fuzhou University, Fuzhou, China, **17** School of Medical Science, Division of Molecular and Gene Therapies, Griffith Health Institute, Griffith University, Gold Coast Campus, Australia, **18** Obstetrics and Gynecology Hospital and Institute of Biomedicine, Fudan University, Shanghai, China

## Abstract

Drug targeting is an active area of research and nano-scaled drug delivery systems hold tremendous potential for the treatment of neoplasms. In this study, a novel cyclodextrin (CD)-based nanoparticle drug delivery system has been assembled and characterized for the therapy of folate receptor-positive [FR(+)] cancer. Water-soluble folic acid (FA)-conjugated CD carriers (FACDs) were successfully synthesized and their structures were confirmed by 1D/2D nuclear magnetic resonance (NMR), matrix-assisted laser desorption ionization time-of-flight mass spectrometer (MALDI-TOF-MS), high performance liquid chromatography (HPLC), Fourier transform infrared spectroscopy (FTIR), and circular dichroism. Drug complexes of adamantane (Ada) and cytotoxic doxorubicin (Dox) with FACD were readily obtained by mixed solvent precipitation. The average size of FACD-Ada-Dox was 1.5–2.5 nm. The host-guest association constant  $K_a$  was  $1,639 \text{ M}^{-1}$  as determined by induced circular dichroism and the hydrophilicity of the FACDs was greatly enhanced compared to unmodified CD. Cellular uptake and FR binding competitive experiments demonstrated an efficient and preferentially targeted delivery of Dox into FR-positive tumor cells and a sustained drug release profile was seen *in vitro*. The delivery of Dox into FR(+) cancer cells *via* endocytosis was observed by confocal microscopy and drug uptake of the targeted nanoparticles was 8-fold greater than that of non-targeted drug complexes. Our docking results suggest that FA, FACD and FACD-Ada-Dox could bind human hedgehog interacting protein that contains a FR domain. Mouse cardiomyocytes as well as fibroblast treated with FACD-Ada-Dox had significantly lower levels of reactive oxygen species, with increased content of glutathione and glutathione peroxidase activity, indicating a reduced potential for Dox-induced cardiotoxicity. These results indicate that the targeted drug complex possesses high drug association and sustained drug release properties with good biocompatibility and physiological stability. The novel FA-conjugated  $\beta$ -CD based drug complex might be promising as an anti-tumor treatment for FR(+) cancer.

**Citation:** Yin J-J, Sharma S, Shumyak SP, Wang Z-X, Zhou Z-W, et al. (2013) Synthesis and Biological Evaluation of Novel Folic Acid Receptor-Targeted,  $\beta$ -Cyclodextrin-Based Drug Complexes for Cancer Treatment. PLoS ONE 8(5): e62289. doi:10.1371/journal.pone.0062289

**Editor:** Caterina Cinti, Institute of Clinical Physiology, c/o Toscana Life Sciences Foundation, Italy

**Received:** December 6, 2012; **Accepted:** March 19, 2013; **Published:** May 2, 2013

**Copyright:** © 2013 Yin et al. This is an open-access article distributed under the terms of the Creative Commons Attribution License, which permits unrestricted use, distribution, and reproduction in any medium, provided the original author and source are credited.

**Funding:** Dr JJJ is supported by a postdoctoral scholarship from the College of Pharmacy, University of South Florida, 12901 Bruce B Downs Blvd., Tampa, Florida. The funders had no role in study design, data collection and analysis, decision to publish, or preparation of the manuscript.

**Competing Interests:** The authors have declared that no competing interests exist.

\* E-mail: szhou@health.usf.edu

## Introduction

Cancer is a leading killer of human beings worldwide, accounting for 7.6 million deaths (around 13% of all deaths) in 2008 [1]. Overall, an estimated 12.7 million new cancer cases and 7.6 million cancer deaths occurred in 2008, with 56% of new cancer cases and 63% of the cancer deaths occurring in the less developed regions of the world [2]. The most commonly diagnosed cancers worldwide are lung (1.61 million, 12.7% of the total), breast (1.38 million, 10.9%) and colorectal cancers (1.23 million, 9.7%). Novel, safe and effective treatments are clearly and urgently needed to curtail these high mortality statistics. The four major modules of cancer treatment include surgery, radiation, chemotherapy and immunotherapy [3]. However, these therapies are only successful when the cancer is detected at an early stage, or limited to certain types of cancer (e.g., leukemia). Due to the inability of detecting cancer at an early stage, most patients present in the advanced stage with extensive local infiltration and metastasis. For advanced tumors, in particular those tumors developed from epithelial tissues such as lung, colon, breast, prostate and pancreas, these therapies are less successful. Chemotherapy represents one of the major means for cancer treatment, which aims to kill tumor cells or to inhibit their proliferation while preserving the normal cells in the body [3]. Chemotherapeutic agents generally have a narrow margin of safety, and are used in combination usually given at a maximum tolerated dose to achieve maximum cancer cell killing [4]. They kill tumor cells by direct cytotoxicity, or activating host immune response, inhibiting the proliferation processes of tumor cells, and inducing apoptosis [5]. However, most patients do not respond to these drugs and they often experience severe adverse effects such as severe diarrhea and loss of hairs. The primary reason for this is because the drug kills both normal and tumor cells due to low drug selectivity and drug levels within tumor cells are too low. Drug resistance and dose-limiting toxicities are the major problems for the success of cancer chemotherapy [6]. In the past decade, nano-scaled, targeted drug delivery has attracted much attention as a means to improve the curative effect of existing chemotherapeutic agents while reducing their adverse effects [7,8]. Recent dramatic developments in nanotechnology have created a myriad of anticancer nano-drugs; however, most current nano-drug systems fall short in ease of purification, reproducibility and batch-to-batch consistency [9,10]. The preparation and characterization of nano-drug formulations especially for aqueous drug complexes remains a major challenge.

The anthracycline glycoside antibiotic, doxorubicin (Dox), is a potent, broad-spectrum anticancer agent that acts by intercalating within DNA and inhibiting DNA synthesis [11]. Dox is often used to treat some leukemias and Hodgkin's lymphoma, as well as cancers of the bladder, breast, stomach, lung, ovaries, thyroid, and soft tissue sarcoma. At the usual chemotherapeutic doses, Dox is cardiotoxic and it may also increase the risk of leukemia especially when it is given at high doses or together with certain other chemotherapeutic agents or radiation therapy [11–16].

The aim of this report is to present a method for synthesizing a novel and effective drug complex for targeted drug delivery (Figure 1). Combining targeting molecules, drug carriers and cytotoxic agents into a complex should guarantee the stability of the conjugate in circulation and insure cleavability to release the drug. The  $\beta$ -CD was vectorized with folic acid (FA) to target folate receptors (FRs) on the tumor cell surface. Dox-containing FR-targeting  $\beta$ -CDs were synthesized by a multi-step reaction in which  $\alpha$ - and  $\gamma$ -amide monomers as well as the di-CD substituted FA carrier were purified and fully characterized by a panel of

spectral techniques. The *in vitro* drug release profile was determined by dialysis and fluorescence measurement, and targeted drug binding *in vitro* was quantitated by flow cytometry and confocal microscopy. The cytotoxicity of the different drug complexes was measured and the biomarkers related to free Dox-induced cardiotoxicity were also examined at the cellular level.

## Materials and Methods

### Chemicals and Reagents

$\beta$ -Cyclodextrin hydrate and cerim (IV) sulphate tetrahydrate were purchased from Acros Organics (Thermo Fisher Scientific, Waltham, MA). Ammonium molybdate (para) tetrahydrate was purchased from Alfa Aesar Inc. (Ward Hill, MA). *p*-Toluenesulfonyl chloride, *N,N*-dicyclohexyl-carbodiimide (DCC), folic acid (FA), *N*-hydroxysuccinimide (NHS), doxorubicin hydrochloride, 1-adamantanecarbonyl chloride, ammonium bicarbonate, sodium azide, triphenylphosphine, 2', 7'-dichlorofluorescein diacetate (DCFH-DA), 5, 5'-dithiobis(2-nitrobenzoic acid) (DTNB), reduced glutathione (GSH), hydrogen peroxide, potassium hydroxide, sodium hydroxide, phosphoric acid, ammonia hydroxide, ninhydrin, hydrochloric acid, iodine, sulfuric acid, acetic acid, deuterium oxide, chloroform-*d*, dimethyl sulfoxide-*d*<sub>6</sub>, and CM sephadex C<sub>25</sub> were all purchased from Sigma-Aldrich Chemicals Co. (St. Louis, MO). Paraformaldehyde was obtained from EMD Chemicals Inc. (Gibbstown, NJ). The bicinchoninic acid (BCA) assay kit was purchased from Pierce (Rockford, IL). CM-H<sub>2</sub>DCFDA was purchased from Invitrogen (Carlsbad, CA). The Pro-prep (TM) Protein extraction kit was purchased from iNtRon Biotechnology Inc. (Kyungki-Do, Korea). The glutathione peroxidase (GPx) assay kit was obtained from BioVision Inc. (Milpitas, CA). Spectra/Por dialysis membrane with a molecular weight cutoff of 3,000 Da was purchased from Spectrum Laboratories (Rancho Dominguez, CA). All solvents for chromatographic isolation were of analytical grade. HPLC-grade acetone, butanol, acetonitrile (ACN), ethyl acetate (EtOAc), hexane, methanol, 1-propanol (1-PA), 2-propanol, dichloromethane (DCM), pyridine, dimethylformamide (DMF), dimethyl sulfoxide (DMSO) and thin layer chromatography plates (1,000  $\mu$ m and 200  $\mu$ m) were purchased from Fisher Scientific Co. (Fair lawn, NJ). Heat-inactivated fetal bovine serum, fetal bovine serum, and newborn calf serum were purchased from Hyclone Laboratories Inc. (Logan, UT). FR and  $\beta$ -actin antibody were purchased from Santa Cruz Biotechnology (Santa Cruz, CA). HRP mouse anti-rabbit IgG monoclonal antibody was purchased from ProSci Inc. (San Diego, CA). Pierce ECL western blotting substrate was purchased from Thermo Fisher Scientific Inc. (Waltham, MA).

### Cells and Cell Culture

JEG-3 and JAR (both derived from human placenta choriocarcinoma), HT-29 (human colon cancer), MCF-7 (human breast cancer), H9C2(2-1) cells (mouse cardiomyocytes) and 3T3 (mouse fibroblast) cell lines were purchased from American Type Culture Collection (ATCC, Rockville, MD). JEG-3 cells were cultured in Dulbecco's modified Eagle medium (DMEM) with 10% newborn calf serum; JAR and MCF-7 cells were cultured in RPMI-1640 with 10% newborn calf serum; HT-29 cells were cultured in McCoy's 5A with 10% newborn calf serum; and 3T3 cells were cultured in DMEM with 10% fetal calf serum. All cell lines were incubated in 5% CO<sub>2</sub> and 90–100% relative humidity at 37°C. Medium renewal was carried out 2–3 times per week, and cells were subcultured when they achieved 80–90% confluence. For slide preparation, 2 × 10<sup>4</sup> cells were plated on 0.7 cm × 0.7 cm Nunc brand chamber slides from Thermo Fisher Scientific (Waltham, MA). Cells were washed three times in phosphate-

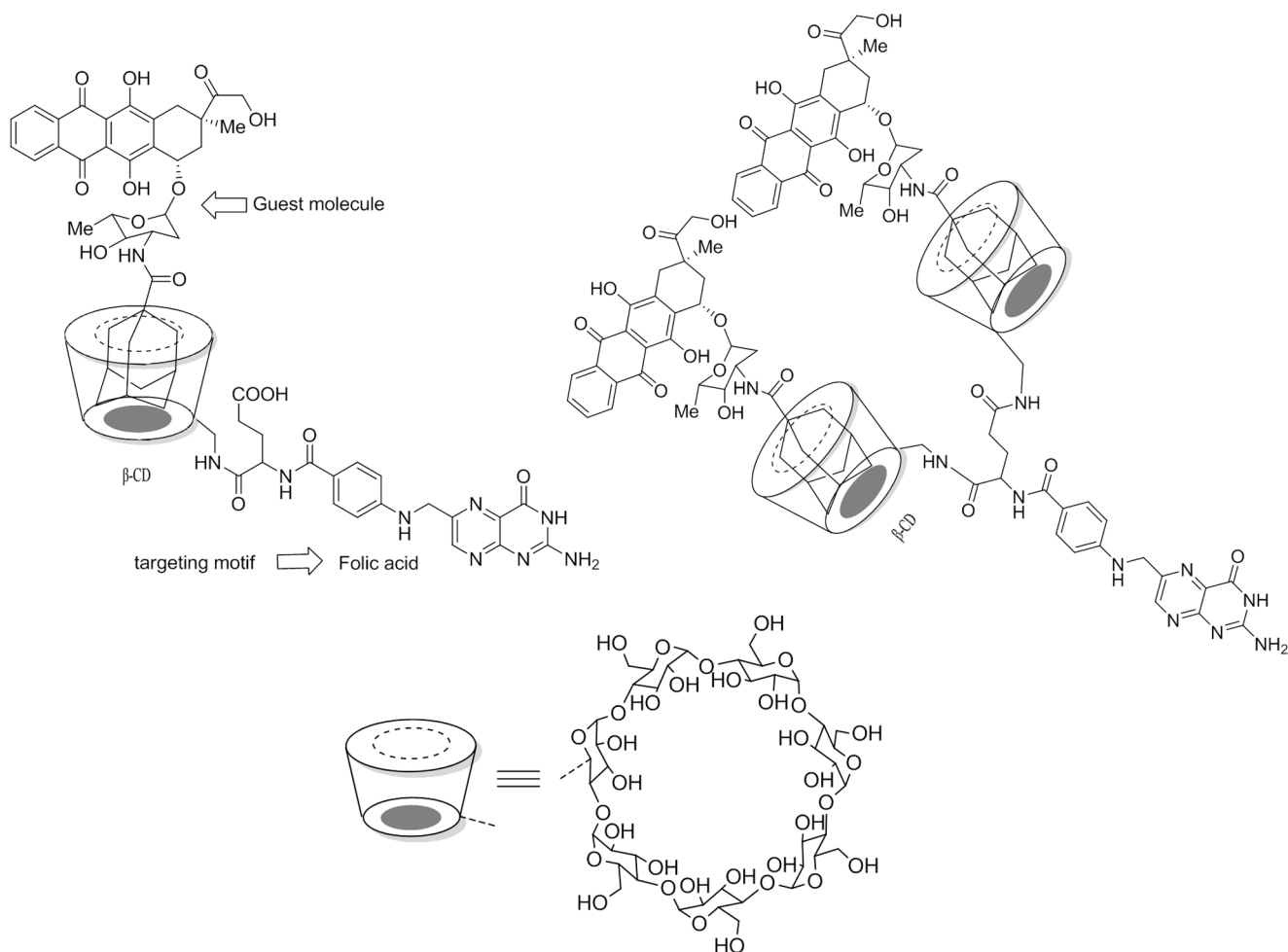


**Figure 1. The chemical structures of FACD-Ada-Dox (a) and FA-diCD-Ada-Dox (b).**  
doi:10.1371/journal.pone.0062289.g001

buffered saline (PBS) and overlaid with Vectashield brand mounting medium containing 4,6-diamidino-2-phenylindole (DAPI) purchased from Vector Laboratories Inc. (Burlingame, CA).

### Western Blot Assay

The protein content was determined using the BCA method after protein extraction from the cells. The expression level of FR in JAR, HT-29, MCF-7 and 3T3 cell lines was determined by Western blot assay. Briefly, cell monolayers were washed with PBS and then the lysates were boiled for 10 min and an aliquot was used to evaluate the protein content by BCA assay. An aliquot of total protein (0.2 mg) was analyzed by 12% sodium dodecyl sulfate polyacrylamide gel electrophoresis (SDS-PAGE). After electroblotting of gels onto polyvinylidene difluoride (PVDF) sheets (Millipore, Bedford, MA), the filters were blocked at room temperature with the Tris-buffered saline Tween-20 (TBST) buffer (10 mM Tris-HCl, pH 8.0, 0.1% Tween 20, and 150 mM NaCl) containing 10% non-fat dry milk and then incubated in TBST buffer overnight at 4°C with a 1:200 dilution of FR antibody and 1:10,000 dilution for  $\beta$ -actin antibody. After washing with TBST buffer, blots were incubated for 1 hr at room temperature with mouse anti-rabbit IgG monoclonal antibody diluted 1:3,000 in TBST buffer and then revealed by enhanced chemiluminescence (ECL).

### Chemical Synthesis of Folic Acid Receptor-Targeted, $\beta$ -Cyclodextrin-Based Drug Complexes

To synthesize mono-6-deoxy-6-(*p*-tolylsulfonyl)- $\beta$ -cyclodextrin (Ts-CD), a solution of *p*-toluenesulfonyl chloride (846.3 mg, 4.44 mmol) in 5 ml ACN was added to 80 ml aqueous solution of  $\beta$ -CD (5.0 g, 4.44 mmol) and NaOH (434.8 mg, 10.8 mmol) dropwise over 15 min. After stirring for 4 hr at 0°C in  $N_2$  atmosphere, the solution was neutralized by adding 0.6 ml of 2.0 N aqueous hydrochloric acid and the product was recrystallized at 4°C overnight, and then washed with acetone. Ts-CD was obtained in a yield of 84.6% (Figure 2 and Figures S1 & S2).

Mono-6-azido-6-deoxy- $\beta$ -cyclodextrin ( $N_3$ -CD) was obtained by the reaction of Ts-CD and sodium azide for 5 hr at 80°C with a yield of 91.5%. Mono-6-deoxy-6-amino- $\beta$ -cyclodextrin ( $NH_2$ -CD):  $N_3$ -CD and triphenyl phosphine were dissolved in DMF, and ammonia solution was added and the solution stirred for 3 days at 50°C. The final solution was recrystallized in acetone to give the compound  $NH_2$ -CD in 79% yield (Figure 2 and Figure S3), which was purified by ion exchange column with deionized water and 0.1 M  $(NH_4)_2CO_3$ .

Ada-COCl was dissolved in anhydrous DCM mixed with  $Et_3N$ , and then stirred at room temperature for 3 hr under  $N_2$ . Doxorubicin hydrochloride was then added, stirred overnight and separated by preparative thin layer chromatography (TLC).

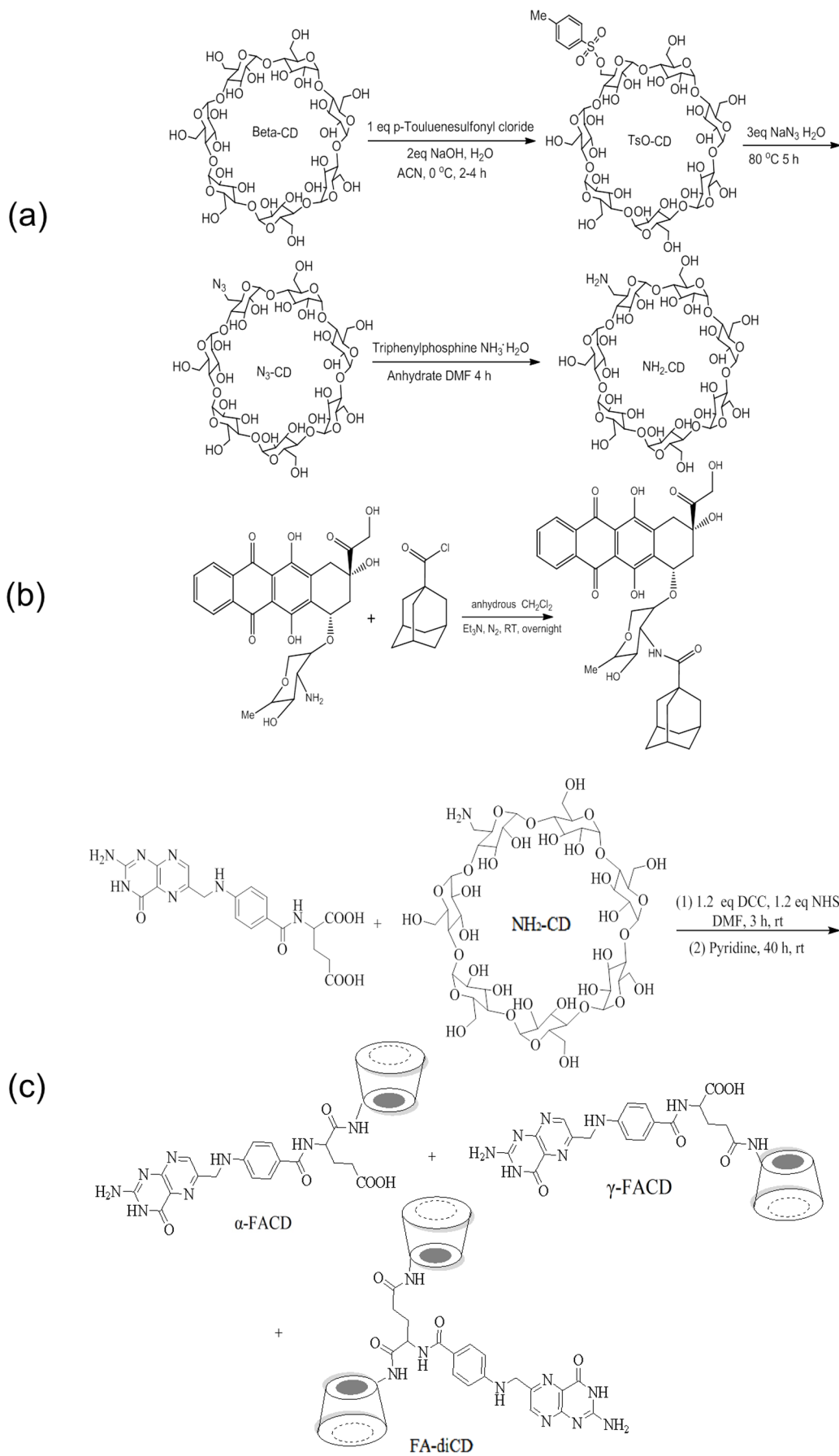


**Figure 2. The reaction schemes to generate Ada-Dox (a), NH<sub>2</sub>-CD (b), and FACDs (c).**  
doi:10.1371/journal.pone.0062289.g002

Ada-Dox was obtained and purified by flash column with a yield of 80.5% (Figure 2 and Figure S4).

A mixture of folic acid (20 mg, 0.045 mmol), 1.2 equivalents of DCC (11 mg, 0.054 mmol) and 1.2 equivalents NHS (6 mg, 0.054 mmol) in anhydrous DMF (5 ml) was stirred at room temperature under a nitrogen atmosphere and in a dark for 3 hr. Thereafter, 50 mg of NH<sub>2</sub>-CD (1 equivalent) and 0.8 ml pyridine were added and the mixture was stirred at room temperature in the dark for 8–40 hr. The reaction mixture was then precipitated with 50 ml of acetone and rinsed sequentially three times with 50 ml of acetonitrile, ethyl acetate, and ethanol to remove hydrophobic side products. The resulting yellow precipitate (48 mg) was collected by centrifugation and dissolved in 20 ml deionized water. A clear aqueous solution (15 ml) was obtained by vacuum filtration, which was dialyzed extensively against deionized water for one week, with dialysis water being renewed every day. The aqueous solution was concentrated down to 5 ml and was chromatographed on a CM sephadex C<sub>25</sub> ion exchange flash column with deionized water and followed by preparative thin liquid chromatography eluted with 1-PA: EtOAc: H<sub>2</sub>O: NH<sub>3</sub>H<sub>2</sub>O (6:1:2.5:1). The products contained the folic acid conjugates and another oily yellow byproduct with polarity similar to the desired product. Finally, the diastereomers were totally purified by recrystallization in acetone three times, and dried in a vacuum oven overnight. This resulted in the products, mono-6-deoxy-6-( $\gamma$ -(2*S*)-2-[[4-[[2-amino-4-hydroxypteridin-6-yl] methyl] amino] phenyl] formamido] pentanedioic acid)- $\beta$ -cyclodextrin ( $\gamma$ -FACD) 11.6 mg (Figures S5 & S5) in 41.6% yield (dark yellow powder), mono-6-deoxy-6-( $\alpha$ -(2*S*)-2-[[4-[[2-amino-4-hydroxypteridin-6-yl] methyl] amino] phenyl] formamido] pentanedioic acid)- $\beta$ -cyclodextrin ( $\alpha$ -FACD) 3.2 mg (Figures S7 & S8) in 11.4% yield (light yellow powder), as well as trace amount of di-mono-6-deoxy-6-(2*S*)-2-[[4-[[2-amino-4-hydroxypteridin-6-yl] methyl] amino] phenyl] formamido] pentanedioic acid)- $\beta$ -cyclodextrin (FA-di-CD) 3.4 mg (Figure S9) in 7.1% yield (Figure 2).

The formation of guest-host inclusion complexes between Ada-Dox and folic acid-conjugated cyclodextrins was prepared by coprecipitation and drying method with 1:1 stoichiometry. FACDs (1 eq) were dissolved in water, and the DMSO solution of Ada-Dox (1 eq) was added to the cyclodextrin solution and then stirred overnight at 4°C followed by partial evaporation. The precipitate was collected by filtration.

### Nuclear Magnetic Resonance (NMR) and Matrix-Assisted Laser Desorption Ionization Time-of-Flight Mass Spectrometer (MALDI-TOF-MS)

High-resolution <sup>1</sup>H NMR spectra were recorded on a digital NMR Spectrospin Bruker Avance 600 MHz and 800 MHz (Bruker BioSpin Co., The Woodlands, TX). The release kinetics of the drugs was measured using a Perkin-Elmer Lambda 2 UV/vis double beam spectrophotometer. Fluorescence microscopy images were obtained with the Applied Precision DeltaVision system (Issaquah, WA) equipped with an Olympus inverted microscope IX 70 (Tokyo, Japan). The image workstation includes SoftWoRx software for digital image acquisition, deconvolution, and optical sectioning.

Mass spectra were obtained by a Bruker Daltonics Autoflex MALDI-TOF (Bruker Daltonics Inc., Billerica, MA), with  $\alpha$ -cyano-4-hydroxycinnamic acid (CHCA) as the matrix (10.0 mg/

ml, from Thermo Scientific Pierce). Data analysis was performed with the mMass program.

### High Performance Liquid Chromatography (HPLC)

HPLC analyses were carried out on an Agilent 1260 Infinity HPLC system (Agilent Technologies Inc., Santa Clara, CA) that included G1312C solvent delivery binary pumps, a G1379B degasser, a G1329B auto-sampler, a G4212B photo-diode array detector, a G1321B Fluorescence detector, and the Chemstation operating software (Rev. B. 04. 03). The HPLC was equipped with an Agilent Eclipse Plus C<sub>18</sub> column with a particle size of 3.5  $\mu$ m and column size of 100 mm $\times$ 4.6 mm, which was placed in a column oven (G1316A) under a constant temperature at 25°C. The mobile phase consisted of acetonitrile and water (Gradient). The column flow rate was set at 1.0 ml/min, while the HPLC pressure was controlled between 260–290 bars.

The HPLC-UV/evaporative light scattering detector (ELSD) and the HPLC-DAD/fluorescence separation conditions were as follows: eluent A, water; eluent B, acetonitrile; gradient, 0–6 min (10–15% B), 6–50 min (15–40% B), 50–60 min (40–80% B), and then equilibrated with 10% B for 8 min at a flow of 1.0 ml/min. ELSD was set at a probe temperature of 70°C, a gain of 7 and the nebulizer gas nitrogen adjusted to 2.5 bars.

### Fourier Transform Infrared Spectroscopy (FTIR)

The instrument used for FTIR analysis was a Perkin-Elmer 1725 series FTIR spectrometer (Perkin-Elmer Co., Norwalk, CT) equipped with a room temperature deuterated triglycine sulfate detector and controlled by a Perkin-Elmer 7300 PC. The software used for collecting the FTIR data was the Spectrum version 5.3.1.

### Circular Dichroism Analysis

Circular dichroism spectra were recorded at 25°C in an Aviv model 215 circular dichroism spectrometer (Aviv Biomedicals Inc., Lakewood, NJ) using a 0.1 cm cell for three scans with 0.1 nm bandwidth. The concentration of the drugs was 50  $\mu$ M in DMF unless otherwise indicated. The Synergy H4 hybrid multi-mode microplate reader was purchased from BioTek Instruments Inc. (Winooski, VT).

### Transmission Electron Microscopy (TEM) and Atomic Force Microscopy (AFM)

The morphology and size of the FACD-Ada-Dox supramolecules were evaluated by transmission electron microscopy (TEM) and atomic force microscopy (AFM). An aqueous solution of FACD-Ada-Dox was directly trickled onto a 300-mesh copper grid and dried in a vacuum oven at 35°C for 4 hr, then images were observed by TEM (JEM 100CX; JEOL Ltd, Tokyo, Japan) with an accelerating voltage of 160 kV. For AFM images, the sample was dissolved in double deionized water (1.0 mg/ml), an aliquot of the solution (5.0  $\mu$ l) was spotted onto a freshly cleaved mica surface and heated at 37°C for 3 hr. Imaging was performed on a Multimode Nanoscope AFM in tapping mode, using a fluid cell, J scanner and 200  $\mu$ m cantilevers with 1 nm Si<sub>3</sub>N<sub>4</sub> tips.

### 3-(4, 5-Dimethylthiazol-2-yl)-2,5-diphenyltetrazolium Bromide (MTT) Assay

JAR, HT-29 and 3T3 cells were seeded in 96-well tissue culture plates and maintained overnight in DMEM medium. Cells were then treated with Dox, Ada-Dox, FACD-Ada-Dox, or NFACD-

Ada-Dox at different concentrations and incubated for 24 hr at 37°C. The absorbance was measured after adding MTT. MTT is reduced by mitochondrial dehydrogenases in living cells to a blue-magenta coloured formazan precipitate. The absorbance of dissolved formazan in the visible region correlates with the number of intact active cells. The cytotoxicity was evaluated with reference to the IC<sub>50</sub> value that was defined as the concentration needed for a 50% reduction of survival based on the survival curves. IC<sub>50</sub> values were calculated from dose-response curves (i.e., cell survival fraction *vs.* drug concentration) obtained in multi-replicated experiments.

### Drug Release Assay

The *in vitro* release profiles and kinetics of the targeting drug FACD-Ada-Dox and prodrug Ada-Dox were determined by a dialysis method. Briefly, 3 ml of aqueous drug was added to 1 ml PBS (pH 7.4, 0.01 M). The mixture was suspended in a dialysis bag (molecular weight cutoff: 3,000 Dal) and dialyzed against 10 ml of PBS containing 50% fetal bovine serum (FBS) at 37°C with gentle shaking for three days. A 20 µl aliquot of the sample was withdrawn from the incubation medium at designated time points and stored frozen for analysis. The released Ada-Dox was quantified by microplate reader at  $\lambda_{EX}$  = 490 nm and  $\lambda_{EM}$  = 600 nm. A calibration curve was prepared using different concentrations of free Ada-Dox.

### Flow Cytometry

Flow cytometric analysis was performed on a FACS (Becton Dickinson Immunocytometry Systems, San Jose, CA) by counting 10,000 events. To evaluate the apoptosis of cells treated with various drugs at equivalent concentrations, Dox, Ada-Dox, FACD-Ada-Dox and NFACD-Ada-Dox at a final concentration of 5.0 µM were added into the prepared 35-mm petri dishes containing  $2 \times 10^5$  HT-29, MCF-7, or JAR cells in 3.0 ml culture medium. The cells were incubated for 2 hr to allow uptake of the drugs. Before analysis, the cells were carefully washed with PBS three times, trypsinized and resuspended in the medium after incubation. The collected cells were re-dispersed in 500 µl of fresh PBS and stained with 20 µl DAPI at 1.0 µM for flow cytometric analysis. The fluorescence of Dox-related molecule was measured with  $\lambda_{EX}$  at 490 nm and  $\lambda_{EM}$  at 600 nm. The untreated cells incubated with DMEM alone (containing 10% FBS, supplemented with 1% of penicillin) were used as the controls.

### Folate Receptor-Binding Competition Assay

In the drug uptake competition assay, JAR cells (FR positive) were seeded into 35-mm petri dishes containing  $5 \times 10^5$  cells and incubated at 37 °C with FACD-Ada-DOX at 2 µM for 5 hr in the presence of FA at 5, 10 or 50 µM. Afterwards, the cells were washed with PBS three times, trypsinized and resuspended in the PBS. The collected cells were re-dispersed and the fluorescence intensities were determined by flow cytometer.

### Confocal Laser Scanning Microscopy

Confocal images were recorded with a PerkinElmer ultraview ERS spinning disk confocal microscope (PerkinElmer Inc., Waltham, MA). JAR or JEG-3 cells were seeded on cover slips in two-well plates, and cultured overnight. Cells were then incubated with or without 5.0 µM drugs for 2 hr. The cells were washed with PBS three times to remove unbound drugs and fixed in 2 ml of 4% paraformaldehyde at room temperature for 15 min. Fixed cells were washed three times and then mounted with medium containing DAPI (1.5 µg/ml). Slides were cured over-

night in the dark. To study the uptake of drugs over 2 hr in cells treated with different drug complexes, the cells were exposed to drugs with different incubation times (15 min increment). The images were collected and analyzed.

### Molecular Docking of the Binding of FA and Its Conjugates to Human Hedgehog Interacting Protein (HHIP)

Unfortunately, the crystal structures of human and animal RCF/SLC19A1, FR/FR $\alpha$ /FLOR1, FR $\beta$ /FLOR2, FR $\gamma$ /FLOR3, FR $\delta$ /FLOR4 and PCFT/SLC46A1 have not been resolved so far. No structures of bacterial and yeast homologs have been reported and thus it is unlikely to build up a homology model. We conducted preliminary docking study of FA and its conjugates to HHIP that contains a FR $\alpha$  domain was examined using the Discovery Studio 3.1 (Accelrys Software Inc., San Diego, CA) as described by us previously [17,18]. Several functional Modules in Discovery Studio 2.1 were applied, including Diverse Conformation Generation, Calculate Molecular Properties, Create Multiple Linear Regression Model, and CDOCKER. The program was run using a Dell optiplex755 server and Chemoffice2002 (CambridgeSoft, Cambridge, MA) was used for compound structural refinement. The crystal structure of HHIP was selected from the Protein Data Bank (<http://www.rcsb.org/pdb/>) with the PDB ID of 2WFT [19] that was found to contain a FR $\alpha$  domain when we searched the Pcam 26.0 database (<http://pfam.sanger.ac.uk/>). The Pfam database is a large collection of protein families, each represented by multiple sequence alignments and hidden Markov models. The molecular dynamics (MD) simulated annealing process was performed using a rigid protein and flexible ligand. The ligand-FR $\alpha$  interactions were computed from either GRID I, GRID II, or the full force field. A final minimization step was applied to each of the ligand's docking poses. During ligand preparation, the duplicate structure was deleted. The options for ionization change, tautomer or isomer generation, Lipinski filter and 3D generator were all set true [20]. After refined with CHARMM, the compounds were docked into the possible binding site of the protein. The docking was carried out with consideration of electrostatic energy and van der Waals (vdW) force, which were softened at different levels during the docking process, but this softening is removed for the final minimization [21]. For each defined vdW or electrostatic probe, the interactions with all protein atoms were stored at these grid points. For ligand atoms located between grid points, a tri-linear interpolation was used to approximate the energies. A harmonic potential with the force constant of 300 kcal/mol was applied outside the grid boundary.

### Determination of Cellular Reactive Oxygen Species (ROS) Levels

The intracellular ROS levels in mouse H9C2(2-1) cells were quantified using CM-H<sub>2</sub>DCFDA as the probe for ROS production [22]. CM-H<sub>2</sub>DCFDA is a chloromethyl derivative of H<sub>2</sub>DCFDA, useful as an indicator for ROS in cells. H9C2(2-1) cells were seeded on a dish at a density of  $3 \times 10^6$  cells per well and cultured in 5% CO<sub>2</sub> at 37°C for 24 hr. The cells were treated with Dox, Ada-Dox, FACD-Ada-Dox, or NFACD-Ada-Dox, and then rinsed with PBS. Afterward, the fluorescence intensity was measured. The drug concentration was 2.0 µM in H9C2(2-1) cells. The control cells were treated with the vehicle DMSO at a final concentration of 0.05% (v/v).

Intracellular ROS levels in mouse 3T3 cells were quantified using the dichlorofluorescein assay [23]. 3T3 cells were seeded on a 96-well plate at a density of  $10^5$  cells per well and cultured in 5%



CO<sub>2</sub> at 37°C for 24 hr. The cells were treated with Dox, Ada-Dox, or FACD-Ada-Dox at 5.0 μM, then the cells were then rinsed by PBS, subsequently 75 μl of PBS, and 25 μl solution of 2',7'-dichlorofluorescein-diacetate (DFCH-DA) at a final concentration 62.5 μM in PBS buffer was added to each well. The fluorescence from each well was measured at 35°C immediately after incorporation of the reagent and every 5 min for 1 hr with 1 sec integration time, using 485 and 535 nm as excitation and emission wavelengths. Recording of the fluorescence intensity with time was used as an index of the individual intracellular levels of ROS in 3T3 cells. The response of the method was checked using a H<sub>2</sub>O<sub>2</sub> curve. Five independent experiments were performed per treatment.

### Measurement of Glutathione Peroxidase (GPx) Activity and GSH Content

The protein content was determined using the BCA method after protein extraction from the cells. The activities of GPx and the content of GSH were scaled to protein content to correct for differences in biomass of the diverse homogenates. The levels of GSH in the cells were determined according to the method of Beutler *et al.* [24] based on the formation of 2-nitro-5-tiobenzoic acid from DTNB in the presence of GSH. In brief, 25 μl of trichloroacetic acid (15%) was added to 50 μl of the homogenate, followed by centrifugation at 13,000 g for 5 min at 4°C. A supernatant aliquot (50 μl) was mixed with 50 μl of 3.4 mM ethylenediaminetetraacetic acid (EDTA) dissolved in PBS, 1 ml of PBS, and 250 μl of DTNB in PBS (20 mg/ml). The absorbance was measured at 412 nm after 15 min and compared to a standard curve of GSH (0.01–0.5 mM). The GPx activity was measured based on the oxidation of GSH by GPx coupled to the disappearance of reduced nicotinamide adenine dinucleotide phosphate (NADPH) by glutathione reductase.

### Statistical Analysis

Data are expressed as the mean ± standard deviation (SD). The comparison of values for multiple treatment groups was performed by one- or two-way analysis of variance (ANOVA) followed by Bonferroni multiple comparison test at  $P < 0.05$ . Differences between two groups were analyzed using unpaired Student's *t*-test. A *P* value of  $< 0.05$  was considered statistically significant.

## Results

### Synthesis of FACDs and FACD-Ada-Dox and Their Structural Determination by Spectral Techniques

The synthetic procedure for FR targeting β-CD based adamantane-Dox supramolecule is depicted in **Figure 2**. To construct the supramolecule, the targeting drug carriers were prepared firstly. Mono-6-amino-6-deoxy-CD (NH<sub>2</sub>-CD) was synthesized as the starting material according to the method of Petter *et al.* [25] with some modifications. Mono-[6-O-(*p*-tolylsulfonyl)]-β-CD (Ts-CD) was prepared by the reaction of β-CD with *p*-toluenesulfonyl, and then Ts-CD was transferred to 6-azido-6-amino-β-CD (N<sub>3</sub>-CD) through nucleophilic reaction. Finally, 6-deoxy-6-amino-β-CD (NH<sub>2</sub>-CD) was obtained by a reaction of N<sub>3</sub>-CD and ammonium hydroxide. The resultant water-soluble FACD isomers (α, γ and double CD substituted folic acid) were prepared by the coupling of NHS activated NH<sub>2</sub>-CD and folic acid using DCC, the FACDs were purified through ion exchange column, dialysis method, and preparative thin layer chromatography and recrystallization. In addition, the guest molecule Ada-Dox was synthesized according to the reaction of

**Figure 2b** in which Dox was grafted to the adamantine through amide bonding.

The resultant water-soluble FACD isomers were prepared and isolated in a multi-step reaction and the structure of each isomer was characterized by 1D/2D NMR including gradient-selected correlation spectroscopy (g-COSY), heteronuclear multiple-bond correlation spectroscopy (HMBC), and heteronuclear multiple-quantum correlation spectroscopy (HMQC), UV spectroscopy, FTIR, HR-MALDI-TOF-MS, and HPLC. The structure of α and γ isomers exhibited the stereochemistry as indicated in **Figure 2c**. The activation energy of diastereomer γ-FACD ( $E_{A\gamma} = 2729.26$  kJ/mol, as modeled by Spartan 08 1. 2. 0) was slightly lower than that of α-FACD ( $E_{A\alpha} = 2,736.52$  kJ/mol). Lengthening the reaction time up to over 48 hr at 40°C favored the formation of α-FACD, which is taken as the thermodynamic product. In contrast, shortening the reaction time to 8 hr at room temperature (about 20°C) resulted in γ-FACD as the dominant product under kinetic control.

The HR-MALDI-TOF-MS spectra of the γ-FACD and α-FACD diastereomers as well as FA-conjugated β-CD dimer (FA-diCD) showed the strong molecular ion peaks of C<sub>61</sub>H<sub>88</sub>N<sub>8</sub>NaO<sub>39</sub> at *m/z* 1,579.414 (intensity 100%), C<sub>61</sub>H<sub>89</sub>N<sub>8</sub>NaO<sub>39</sub> at *m/z* 1,580.255 (intensity 100%), and C<sub>103</sub>H<sub>158</sub>N<sub>9</sub>NaO<sub>72</sub> at *m/z* 2,695.992 (intensity 100%), respectively (**Figure 3** and **Figures S10, S11 & S12**). The enhanced polarity was observed in an order of α-FACD, γ-FACD, and FA-diCD with *R<sub>f</sub>*-values of 0.53, 0.30, and 0.23, respectively, when developed in 1-propanol/ethyl acetate/water/ammonium hydroxide (3:1:2:1, v/v). The preferential product, γ-FACD, might result because of its longer linkage and less steric stress than α-substituted, and because the former had a slightly higher energy than the later isomer.

The spectral data of FACDs were obtained: <sup>1</sup>H NMR (800 MHz, D<sub>2</sub>O, δ) of γ-FACD: 8.43 (s, NH<sub>2</sub>), 7.26 (m, Ar, 2H), 6.48 (m, Ar, 2H), 3.39–3.71 ppm (m, CH, 56H); <sup>13</sup>C NMR (201 MHz, D<sub>2</sub>O, δ): 217.76, 183.91, 179.67, 177.55, 169.66, 168.99, 157.44, 153.21, 130.62, 123.96, 114.20, 104.15, 86.45, 83.39, 75.78, 74.25, 62.43, 56.92, 48.37, 42.88, 32.87, and 26.14 ppm. IR (KBr): ν = 2,972 (w), 2,907 (w), 1,026 (s), 971 439 (m), 401 cm<sup>-1</sup> (m); UV-vis (H<sub>2</sub>O): λ<sub>max</sub> (ε) = 320, 287, 269, 238 nm; HRMS (MALDI-TOF, *m/z*): [M]<sup>+</sup> calculated for C<sub>61</sub>H<sub>88</sub>N<sub>8</sub>NaO<sub>39</sub>, 1,579.50; observed, 1,579.414 (intensity 100%).

<sup>1</sup>H NMR (800 MHz, D<sub>2</sub>O, δ) of α-FACD: 8.33 (s, NH<sub>2</sub>), 7.55 (m, Ar of FA), 6.33 (m, Ar of FA), 4.89, 4.65, 3.42–3.72 ppm (m, CH of CDs); <sup>13</sup>C NMR (201 MHz, D<sub>2</sub>O, δ): 194.67, 185.70, 115.20, 95.99, 4.31, 93.98, 86.36, 85.41, 85.09, 81.11, 73.80, 56.24, 54.97, 53.62, 38.35, 36.37, and 35.73. IR (KBr): ν = 2,972 (w), 2,907 (w), 1,026 (s), 401 cm<sup>-1</sup> (m); UV-vis (H<sub>2</sub>O): λ<sub>max</sub> (ε) = 281, 205 nm; HRMS (MALDI-TOF, *m/z*): [M+H]<sup>+</sup> calculated for C<sub>61</sub>H<sub>88</sub>N<sub>8</sub>NaO<sub>39</sub>, 1,580.51; observed, 1,580.255 (intensity 100%).

<sup>1</sup>H NMR (600 MHz, D<sub>2</sub>O, δ) of FA-diCD: 8.33 (s, NH<sub>2</sub>), 7.36 (m, Ar of FA), 6.49 (m, Ar of FA), 4.90 ppm, 3.36–3.76 ppm (m, CH of CDs). IR (KBr): ν = 2,972 (w), 2,907 (w), 439 (m), 401 cm<sup>-1</sup> (m); UV-vis (H<sub>2</sub>O): λ<sub>max</sub> (ε) = 281 (5000), 252 nm (12000); HRMS (MALDI-TOF, *m/z*): [M+H]<sup>+</sup> calculated for C<sub>103</sub>H<sub>158</sub>N<sub>9</sub>NaO<sub>72</sub>, 2,695.89; observed, 2,695.992 (intensity 100%).

The structure of the isomers was further identified based on the J-couplings of the protons, and the g-COSY NMR spectra of γ- and α-FACD in D<sub>2</sub>O exhibited two pairs (solid circles in **Figure 2**) of correlated peaks between H<sub>a</sub> and H<sub>b</sub>. The spectra in (a) and (b) clearly showed dominant signals for one isomer and only trace signals for the other. This confirmed the successful preparation, separation and identification of the novel FA-conjugated CD isomers and dimmer. In addition, the UV absorption spectra of

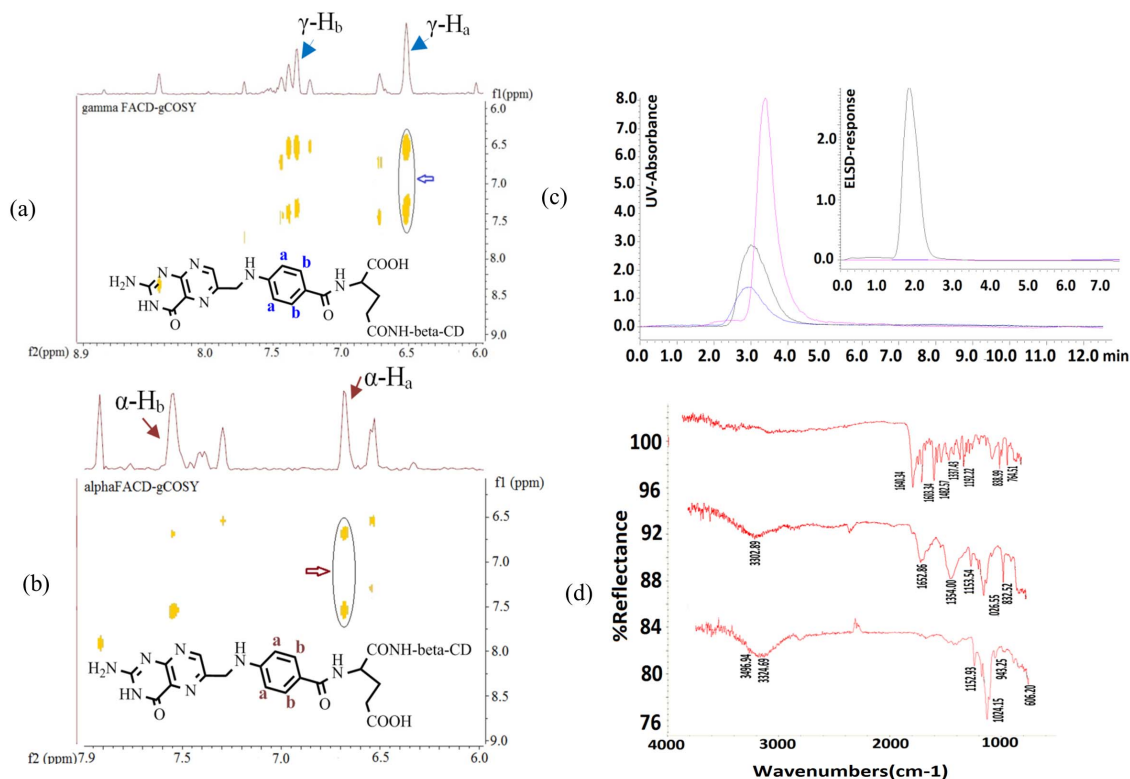


**Figure 3. The g-COSY NMR (600 MHz, D<sub>2</sub>O, T = 298 K), UV/ELSD and FTIR spectra of the  $\beta$ -CD, NH<sub>2</sub>-CD, and  $\gamma$ - &  $\alpha$ -FACDs.** The NMR spectra show two pairs of correlated peaks (solid circle) between aromatic protons ( $\gamma$  substituted FACD protons in blue in Plot a and  $\alpha$ -FACD in red in Plot b) of folic acid framework labeled with a and b. Plot c shows the HPLC-UV and ELSD chromatograms of  $\beta$ -CD (black), NH<sub>2</sub>-CD (blue) and  $\gamma$ -FACD (purple). Plot d illustrates the FTIR spectra of FA (top),  $\gamma$ -FACD (middle) and NH<sub>2</sub>-CD (bottom) (d). doi:10.1371/journal.pone.0062289.g003

the compounds  $\alpha/\gamma$ -FACD as well as FA-diCD all possessed main characteristic FA absorption bands at 281 nm (strong) and 360 nm (medium) with red shifts at 205 nm compared with the UV spectra of native FA (Figure 4f). In the functional region of the FTIR spectrum of FACD (Figure 3d), two broad bands at 3,330 cm<sup>-1</sup> and 3,180 cm<sup>-1</sup> were observed and were assigned to the stretching vibrations of different hydroxyl groups in the  $\beta$ -CD framework involved in hydrogen bonds of different strength; the N-H stretching in the FA residue of FACD contributed as well.

Additionally, the FTIR spectrum (Figure S13) displayed a number of characteristic absorption bands occurring at 1,650, 1,605, 1,390, 1,260, 1,006, and 802 cm<sup>-1</sup> in both the functional and fingerprint regions in which the band at 1,650 cm<sup>-1</sup> belongs to the C=O bond stretching vibration of the -CONH<sub>2</sub> group. The band at 1,605 cm<sup>-1</sup> related to the bending mode of NH-vibration; 1,383 cm<sup>-1</sup> were assigned to the CH<sub>3</sub> symmetrical deformation mode; and the peak at ~800 cm<sup>-1</sup> corresponded to the wagging of the saccharide structure of  $\beta$ -CD. These observations provided further evidence for successful FA conjugation with  $\beta$ -CD.

The coupled HPLC/DAD-ELSD in gradient-elution mode was applied to simultaneous quantification of the resulting FA conjugates and drug complexes (Figure 3c and Figure S14).  $\beta$ -CD, NH<sub>2</sub>-CD and  $\gamma$ -FACD were characterized with t<sub>R</sub> values of 3.0, 3.1, and 3.8 min, respectively.

We conducted circular dichroism analyses for the binding ability, and tested native  $\beta$ -CD at 1.0 mM and at its saturated concentration in DMF (~40 mg/ml), Ada-Dox, FACD, and FACD-Ada-Dox at 1.0 mM in DMF with the cutoff of <265 nm. The final spectra were the average of three scans obtained after

subtracting the spectra of the blank DMF. CD and FA-modified CD displayed ignorable signals, and no obvious spectral change was observed before adding the guest molecule. However, we observed a significant intensity decrease for FACD-Ada-Dox drug complex from 265 to 450 nm in comparison with Ada-Dox prodrug for both positive and negative Cotton effect. Specifically, there were negative and positive extrema at 290 and 350 nm at which molar ellipticity changed by the value of 9.314 and 5.228 deg·cm<sup>2</sup>/dmol, respectively. The association constant,  $K_a$ , was calculated as 1,639 M<sup>-1</sup> by Scatchard plotting method using Prism 5 (GraphPad Software Inc., La Jolla, CA).

#### Particle Size of FACD-Ada-Dox

FACD-Ada-Dox were evaluated by transmission electron microscopy (TEM) (Figure 5a) and atomic force microscopy (AFM) (Figure 5b). The average FACD-Ada-Dox size of the supramolecule was 1.5~2.5 nm and the particles were well dispersed as observed from the TEM and AFM images.

#### In vitro Release Profiles of the Drug Complexes

The release profiles of Ada-Dox from Ada-Dox and FACD-Ada-Dox are shown in Figure 6a & b. The amount of released Ada-Dox was quantified using a validated fluorescence method. When Ada-Dox was loaded, Ada-Dox was rapidly released by 27.6% in 30 min and 56.9% in 150 min, with much slower release thereafter and up to 89.6% in 110 hr. The release of Ada-Dox from FACD-Ada-Dox was 2.0~2.8 fold slower than that when Ada-Dox was loaded ( $P < 0.01$  or 0.001). After 30 min of incubation, 11.8% of Ada-Dox was released and only 25.8% of

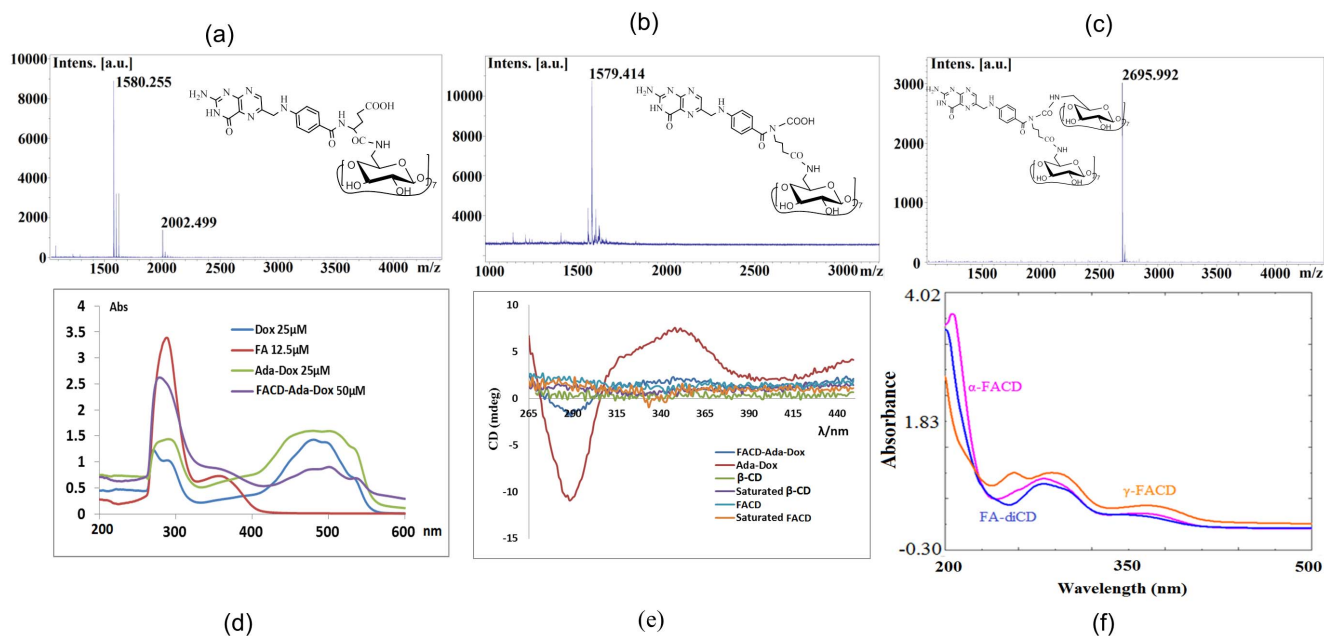


**Figure 4. The HR-MALDI-TOF, UV, and circular dichroism spectra of Dox, Ada-Dox, FA,  $\alpha$ - &  $\gamma$ -FACD, FA-diCD, and FACD-Ada-Dox.** Plots a, b, & c show the MALDI-TOF spectra of  $\alpha$ -FACD,  $\gamma$ -FACD and FA-diCD, respectively. Plot d shows the UV spectra of Dox, Ada-Dox, FA, and FACD-Ada-Dox in DMF. Plot e illustrates the circular dichroism spectra of Ada-Dox,  $\beta$ -CD, FACD and FACD-Ada-Dox in the far and near UV region in DMF at 20°C in the near and far UV (e). Plot f displays the UV spectra of  $\alpha$ - &  $\gamma$ -FACD.  
doi:10.1371/journal.pone.0062289.g004

Ada-Dox was released from FACD-Ada-Dox after 150 min of incubation. After 150 min, Ada-Dox was continuously and slowly released up to 110 hr. The released drug was 33.8%, 40.5%, and 60.2% after FACD-Ada-Dox was incubated for 10, 60, and 110 hr, respectively.

We also calculated the kinetic parameters when the drug release was calculated up to 4 hr using the one-phase exponential decay model (**Figure 6**). The  $K_d$  values were 0.77 and 0.17  $\text{hr}^{-1}$  for

Ada-Dox and FACD-Ada-Dox, respectively. The half-lives were 0.90 and 4.03 hr, respectively. These data clearly demonstrate that Ada-Dox release from FACD-Ada-Dox is significantly slower than Ada-Dox; the host molecule (FACD) retains the guest molecule (Ada-Dox).

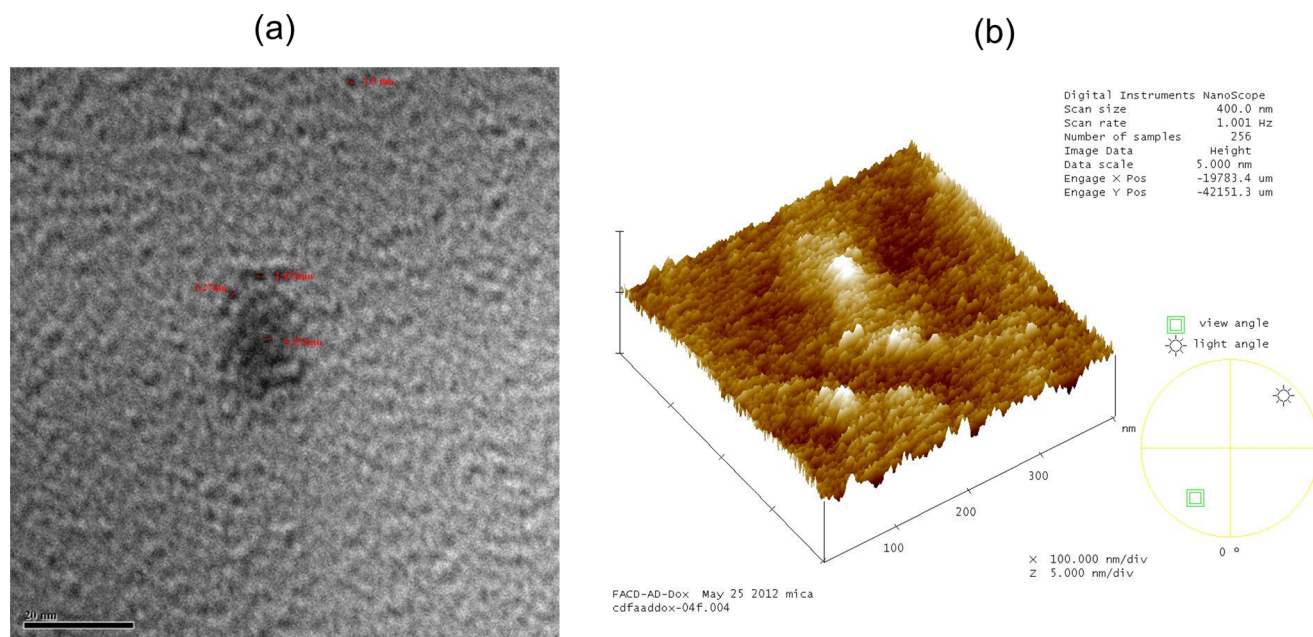


**Figure 5. The TEM (a) and AFM (b) images of FACD-Ada-Dox molecules.**  
doi:10.1371/journal.pone.0062289.g005

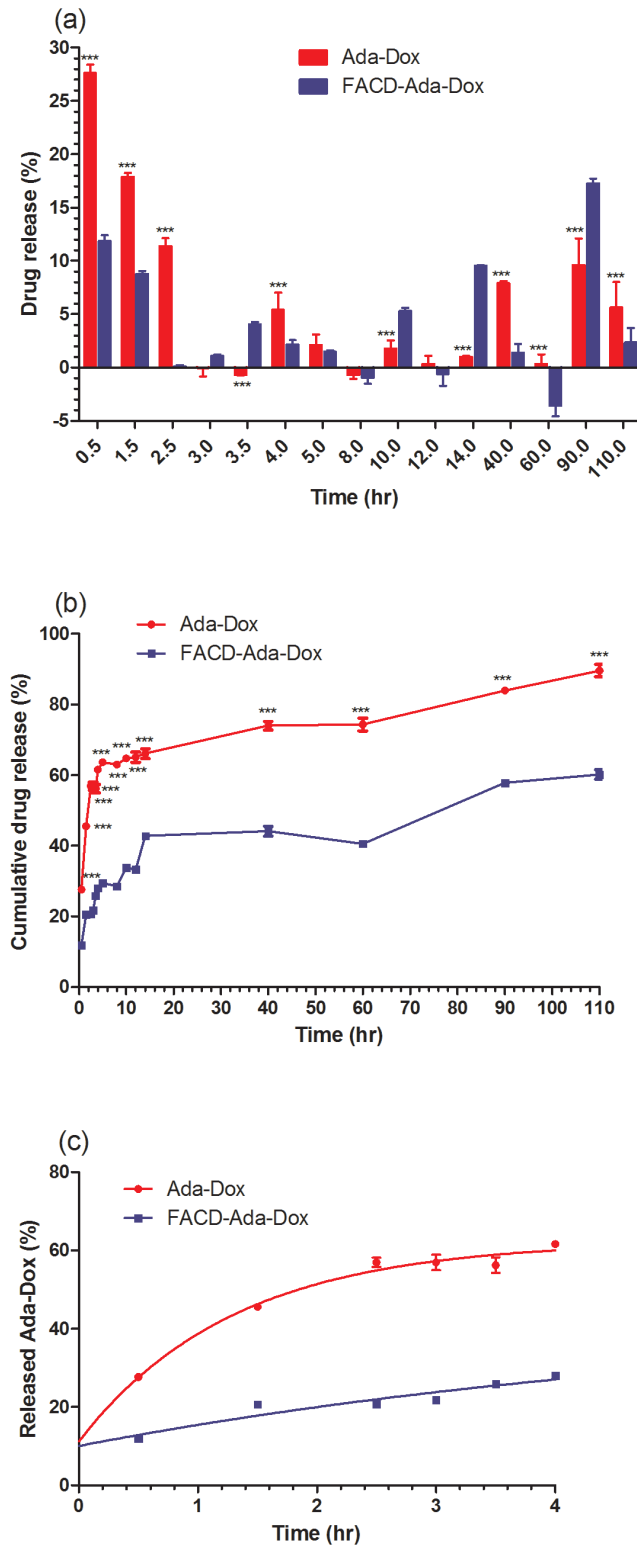


**Figure 6. The drug release profiles of Ada-Dox and FACD-Ada-Dox.** Plots a and b show the absolute and cumulative drug release profiles, respectively. Plot c illustrates the release kinetics and best fit of curves when drug release was calculated up to 4 hr only. The release of Ada-Dox was determined by a dialysis method. The released Ada-Dox was quantified by microplate reader at  $\lambda_{EX} = 490$  nm and  $\lambda_{EM} = 600$  nm. A calibration curve was prepared using different concentrations of free Ada-Dox. \*\*\* $P < 0.001$ . doi:10.1371/journal.pone.0062289.g006

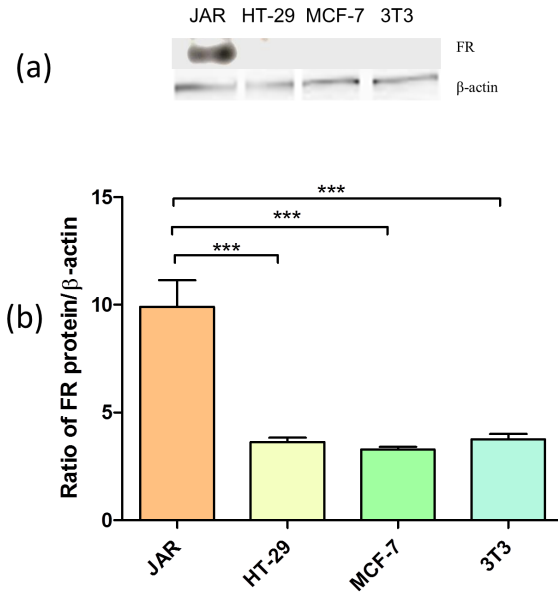


**Figure 7. The folate receptor expression levels in JAR, HT-29, MCF-7 and 3T3 as determined by Western blot assay.** An aliquot of total protein (0.2 mg) was analyzed by 12% SDS-PAGE. After electroblotting of gels onto PVDF sheets, the filters were blocked with TBST buffer containing 10% non-fat dry milk and then incubated in TBST buffer overnight at 4°C with a 1:200 dilution of FR antibody and 1:10,000 dilution for  $\beta$ -actin antibody. After TBST washing, blots were incubated for 1 hr with mouse anti-rabbit IgG monoclonal antibody diluted 1:3,000 in TBST buffer and then revealed by ECL. \*\*\* $P < 0.001$ . doi:10.1371/journal.pone.0062289.g007

#### Expression of FR Protein in Different Cells

The folate receptor expression in JAR, HT-29, MCF-7 and 3T3 was determined by Western blot assay (Figure 7). The FR expression levels in the cell lines tested were significantly different. JAR cells expressed the highest level of FR, while HT-29 and MCF-7 cells had negligible expression of FR ( $P < 0.001$  vs JAR cells).

#### Cytotoxicity of the Drug Complexes in FR(+) JAR and FR(-) HT-29 and 3T3 cells

To examine how the conjugation of Dox with Ada, FACD and other molecule affected its cytotoxicity, we compared the proliferation of human FR(+) JAR and FR(-) human colon cancer HT-29 cells as well as fibroblast 3T3 cells treated with the drug complexes using the MTT assay. The MTT results are summarized in Table 1 and display in Figure 8.

Among all drugs tested, the free Dox showed the lowest  $IC_{50}$  value in all cells when incubated for 24 hr. The conjugation of Dox with FA greatly improved its cytotoxicity in comparison with the prodrug Ada-Dox and non-targeting drug complex, NFACD-Ada-Dox, specifically to FR(+) JAR cells. It led to 2.26 and 12.36 fold decreases in the  $IC_{50}$  values to Ada-Dox and NFACD-Ada-Dox, respectively, and that would be significant in a clinical context. Meanwhile, FA, CD, adamantane, and the carrier FACD barely showed cytotoxicity to all these cells tested. The ability of FACD-Ada-Dox to kill FR(+) cancer cell-compared to NFACD-Ada-Dox indicates that FA-targeted cyclodextrin complexes deliver their Dox prodrug cargos selectively to cancer cells overexpressing FR.

**Table 1.** The cytotoxicity of various drug complexes against human JAR, HT-29 and mouse 3T3 cells when incubated for 24 hr.

IC <sub>50</sub> (μM)	Dox	Ada-Dox	FACD-Ada-Dox	NFACD-Ada-Dox
JAR	0.51±0.04	20.85±0.07 (40.88) <sup>a</sup>	9.22±0.03 (18.08) <sup>b</sup>	114.20±0.06 (223.92) <sup>b</sup>
HT-29	0.79±0.09	9.8±0.06 (12.41) <sup>a</sup>	16.65±0.09 (1.69) <sup>b</sup>	112.10±0.11 (11.43) <sup>b</sup>
3T3	0.39±0.02	78.6±0.03 (201.54) <sup>a</sup>	1770.00 (4538.46) <sup>b</sup>	>10 <sup>3</sup> (>2597.40) <sup>b</sup>

Data are the mean ± SD of at least three independent experiments. The data in the brackets stand for fold change against the treatment with free Dox.

<sup>a</sup>*P*<0.01, vs free Dox; <sup>b</sup>*P*<0.01, vs Ada-Dox; by one-way ANOVA followed by Bonferroni multiple comparison test.

doi:10.1371/journal.pone.0062289.t001

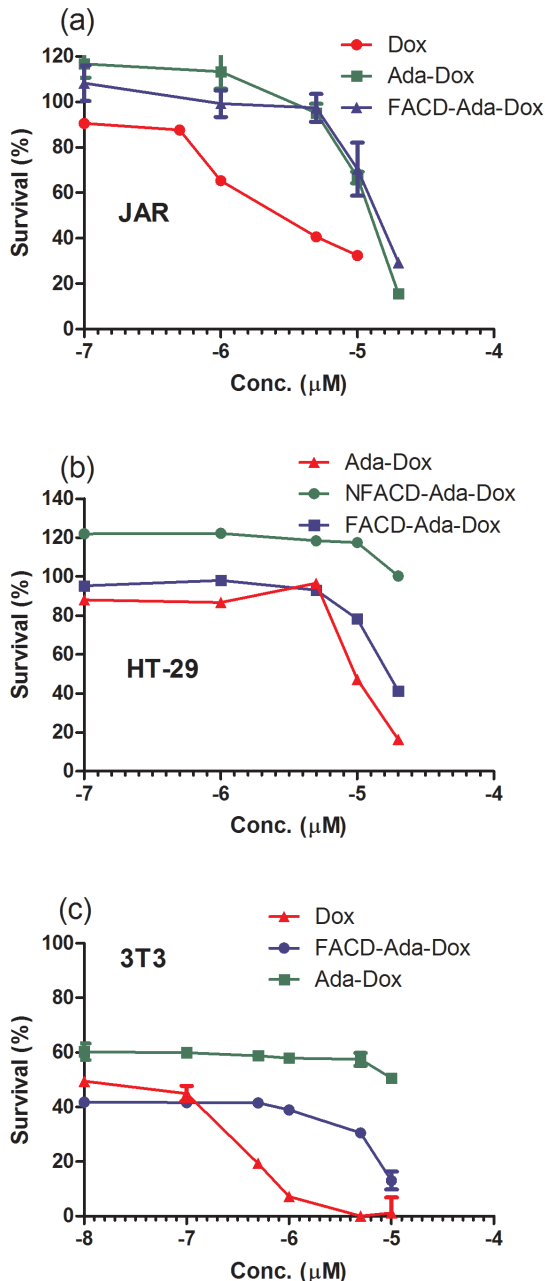


**Figure 8.** The cytotoxicity of the drug complexes to JAR, HT-29 and 3T3 cells based on MTT assay. Data are the mean ± SD of at least three independent experiments. doi:10.1371/journal.pone.0062289.g008

### Uptake of the Drug by HT-29, MCF-7, and JAR cells

The Dox-induced fluorescence intensity in HT-29, MCF-7, and JAR cells treated with Dox, Ada-Dox, FACD-Ada-Dox or NFACD-Ada-Dox was quantitatively determined by flow cytometry with the DAPI-stained cell count for normalization. **Figure 9** illustrates the Dox-related fluorescence intensity when treated with different drugs by flow cytometry. **Table 2** shows the ratio of Dox-related fluorescence intensity in HT-29, MCF-7 and JAR cells treated with different drugs. The data from flow cytometric analysis indicated remarkable differences in Dox-related fluorescence intensity when treated with different drugs in HT-29, MCF-7 and JAR cells (**Figure 10**). In HT-29 cells, treatment with FACD-Ada-Dox significantly resulted in higher Dox-related fluorescence intensity than Dox, Ada-Dox or NFACD-Ada-Dox, with a ratio of 1.70, 1.85 and 2.09, respectively (*P*<0.001). In MCF-7 cells, FACD-Ada-Dox also showed the highest Dox-related fluorescence intensity among all four drugs tested, with a ratio of 1.63, 1.87, and 1.98 over Dox, Ada-Dox and NFACD-Ada-Dox, respectively. In JAR cells overexpressing FR, both FACD-Ada-Dox and Ada-Dox produced significantly higher Dox-related fluorescence intensity compared to Dox and NFACD-Ada-Dox. The ratio of Dox-related fluorescence intensity in JAR cells treated with FACD-Ada-Dox over NFACD-Ada-Dox was 7.31. These results suggest that FR-targeted FACD-Ada-Dox enhanced cellular uptake of the drug, probably through FR-mediated endocytosis.

The data from the competition assay in JAR cells (FR positive) are shown in **Figure 11**. Our flow cytometric analysis showed that folic acid at 5, 10 or 50 μM significantly inhibited FACD-Ada-Dox uptake in JAR cells (*P*<0.01 or 0.001), with an FA concentration of 5 μM causing a maximum inhibition of drug uptake. Increasing the FA concentration to 10 or 50 μM caused a lower inhibitory effect on drug uptake, but there was no statistical significance. These data suggests that FACD-Ada-Dox is internalized through FR-mediated mechanism.

### Uptake and Subcellular Distribution of the Drug in FR(+) JAR and JEG-3 Cells

The endocytotic uptake of FACD-Ada-Dox by FR(+) JAR cells is demonstrated in **Figure 12**. The JAR cells were cultured in drug-containing medium (5.0 μM) for 2 hr followed by paraformaldehyde fixation and staining with DAPI (in blue). Specific patterns of drug accumulation were observed for Dox and Ada-Dox (in red). The prodrug Ada-Dox demonstrated both cytoplasmic and nuclear localization and this differs from the predominant accumulation of free Dox in the nuclei. Dox was observed to be inside the cell after 30 min of incubation at 37°C. Obviously, fluorescence intensity indicates targeting drug internalize much more drug than non-targeting drug.

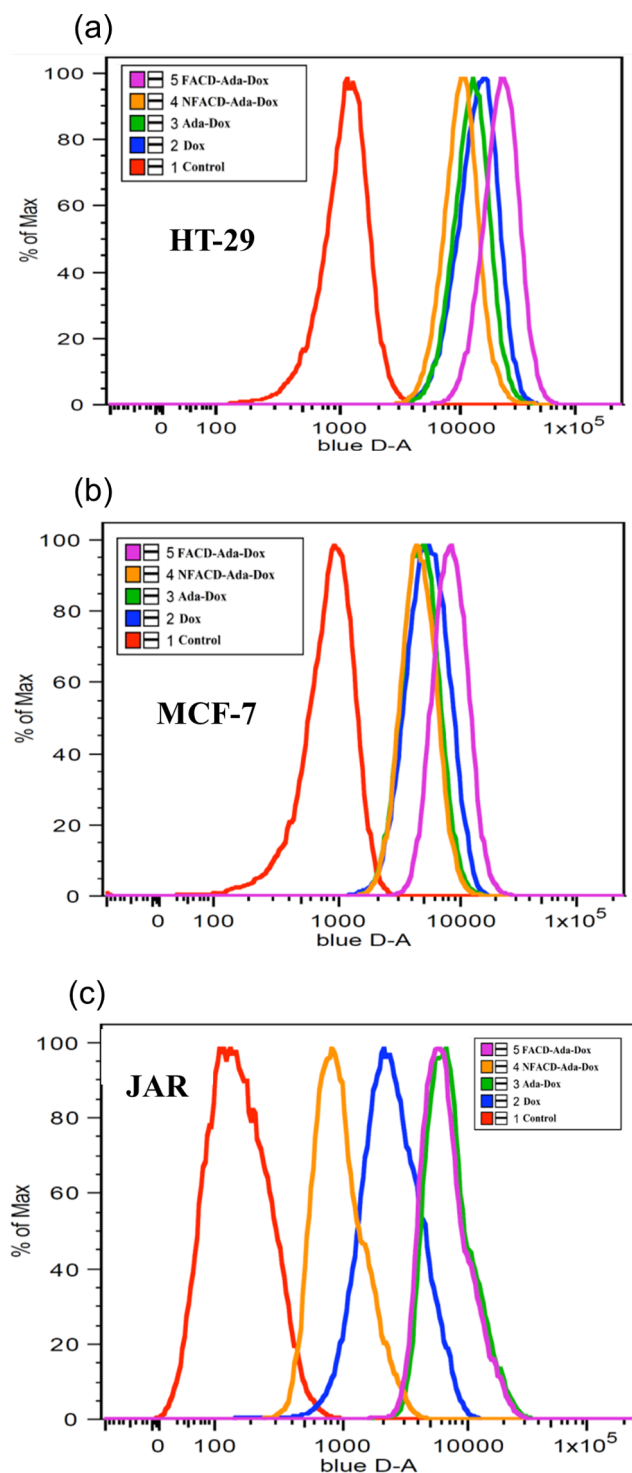


**Figure 9.** Flow cytometric analyses of the Dox-related fluorescence intensity in HT-29 (a), MCF-7 (b) and JAR cells (c) treated with free Dox (blue), Ada-Dox (green), FACD-Ada-Dox (magenta), and NFACD-Ada-Dox (orange). Cells were cultured in the presence of drugs (5  $\mu$ M) at 37°C with 5% CO<sub>2</sub> for 2 hr. Cells incubated with DMEM alone were used as the control (red). doi:10.1371/journal.pone.0062289.g009

#### Binding Modes of FA and Its Conjugates to HHIP

The 2WFT structure of HHIP was used in our docking studies. FA could readily be docked into the possible binding site of HHIP

containing a human FA $\alpha$  domain, with a CDOCKER interaction energy of  $-44.53$  kcal/mol (Figure 13). At least three H-bonds were formed with Pro291, Asp398, and Arg410 each. Arg410 also formed charge interaction with FA. When FA was conjugated with a  $\beta$ -CD molecule, the conjugate FACD could be docked into the possible binding site of FR $\alpha$ , with a CDOCKER interaction energy of  $-95.98$  kcal/mol. The binding involved the formation of at least 11 H-bonds and 2  $\pi$ - $\pi$  stacks between FA with Arg394. FACD formed H-bonds between Ser411 and the FA moiety, and between Asn292, Pro291, Lys295, or Asp398 and the  $\beta$ -CD moiety (Figure 13). Interestingly, Ada-Dox was able to be docked into the possible binding site of HHIP containing a human FA $\alpha$  domain, with an H-bond resulting from the Dox moiety and Lys295 (Figure 13).

#### ROS Accumulation, GPx activity and GSH Content in H9C2(2-1) Cardiomyocytes and 3T3 Fibroblasts Treated with the Drug Complexes

In mouse H9C2(2-1) cells, treatment with Dox at 2.0  $\mu$ M for 18 hr only slightly increased the production of ROS by 8.8% ( $P>0.05$ ), but significantly decreased the GPx activity by 69.0% and the content of intracellular GSH by 92.0% ( $P<0.001$ , Figure 14 & Table 3). It appeared that Dox might mainly induce the production of other radical species rather than ROS, which considerably consumed intracellular GSH and suppressed GPx activity.

Treatment of H9C2(2-1) cells with Ada-Dox, FACD-Ada-Dox or NFACD-Ada-Dox significantly reduced ROS accumulation compared to cells treated with free Dox or 0.05% DMSO ( $P<0.001$ ) (Figure 14a). The GPx activity was increased 337.1% ( $P<0.001$ ), 80.0% ( $P>0.05$ ) and 177.2% ( $P<0.01$ ) in H9C2(2-1) cells treated with Ada-Dox, FACD-Ada-Dox, or NFACD-Ada-Dox, respectively, compared to cells treated with free Dox. When compared to cells treated with the control vehicle 0.05% DMSO, treatment of H9C2(2-1) cells with Ada-Dox increased GPx activity by 35.4% ( $P>0.05$ ), while the GPx activity was significantly decreased by 44.4% in cells treated with FACD-Ada-Dox ( $P<0.05$ ). NFACD-Ada-Dox only slightly reduced the GPx activity compared to the control cells (14.1%,  $P>0.05$ ). Consistently, treatment of H9C2(2-1) cells with Ada-Dox, FACD-Ada-Dox or NFACD-Ada-Dox increased intracellular GSH levels 19.1, 11.7 and 12.0 folds, respectively, compared to cells treated with free Dox ( $P<0.001$ ), respectively, compared to cells treated with 0.05% DMSO only, treatment of H9C2(2-1) cells with Ada-Dox, FACD-Ada-Dox or NFACD-Ada-Dox increased intracellular GSH levels 153.4%, 60.8% and 64.2%, respectively ( $P<0.01$  or 0.001). These findings indicate that conjugating of Ada to Dox or FACD to Ada-Dox reduced the ROS-inducing ability of Dox. Compared to the non-targeted NFACD-Ada-Dox, FACD-Ada-Dox protected mouse cardiomyocytes to a lesser extent in terms of GPx and GSH recovery. This can be explained by increased cytotoxicity due to low expression of FRs in cardiomyocytes exposed to FACD-Ada-Dox.

In mouse 3T3 fibroblast cells, treatment with Dox at 5.0  $\mu$ M over 60 min significantly induced the production of ROS (Figure 15). The ROS level was decreased by 19.5% and 17.5% when treated with Ada-Dox or FACD-Ada-Dox, respectively ( $P<0.05$ , Figure 15 & Table 3), compared to cells treated with free Dox. Dox treatment significantly decreased GPx activity and GSH content. The GPx activity and GSH content in 3T3 cells treated with FACD-Ada-Dox increased by 26.4% and 43.4%, respectively, compared to control cells treated with free Dox. The prodrug Ada-Dox reduced the ROS production in 3T3 cells by

**Table 2.** Ratio of apoptotic cell counts in HT-29, MCF-7 and JAR cells treated with four different drugs determined by flow cytometry.

Cell type	Ratio				
	FACD-Ada-Dox: NFACD-Ada-Dox	FACD-Ada-Dox: Ada-Dox	FACD-Ada-Dox: Dox	NFACD-Ada-Dox: Ada-Dox	Ada-Dox: Dox
HT-29	2.09±0.04***	1.85±0.04***	1.70±0.04***	0.88±0.05	0.87±0.04*
MCF-7	1.98±0.05***	1.87±0.05***	1.63±0.04***	0.95±0.05	0.86±0.05
JAR	7.31±0.34***	0.94±0.06	2.63±0.08***	0.13±0.30***	2.78±0.11***

\* $P<0.05$ ; \*\*\* $P<0.001$ ; by one-way ANOVA followed by followed by Bonferroni multiple comparison test.  
doi:10.1371/journal.pone.0062289.t002

19.5%, but did not alter the GPx activity and GSH content, compared to cells treated with free Dox. Compared to the treatment with Dox or Ada-Dox, both FACD-Ada-Dox and NFACD-Ada-Dox significantly increased the GPx activity and GSH content ( $P<0.05$ ) in 3T3 cells. Since 3T3 cells lack FR expression, the recovering ability of FACD-Ada-Dox and NFACD-Ada-Dox for GPx and GSH is comparable.

## Discussion

A variety of receptors have been identified as markers for carcinomas. FA is a hydrophilic B-complex vitamin which plays an

essential role in mammalian cell survival by participating in the biosynthesis of purines, thymidylate, and certain amino acids [26]. Leucovorin (5-formyl-tetrahydrofolate) and reduced folates (e.g. 5-methyl-tetrahydrofolate) are precursors of one-carbon donors in the *de novo* biosynthesis of purines and thymidylate. FA and its derivatives can cross cells by three mechanisms: a) the reduced folate carrier (RFC/SLC19A1), a bidirectional anion exchanger that has a high affinity for reduced folate co-factors and antifolates (e.g. methotrexate), but a low affinity for FA; RFC can take up folate cofactors and export various organic anions, including thiamine pyrophosphate; b) the folate receptor- $\alpha$  (FR $\alpha$ /FR/

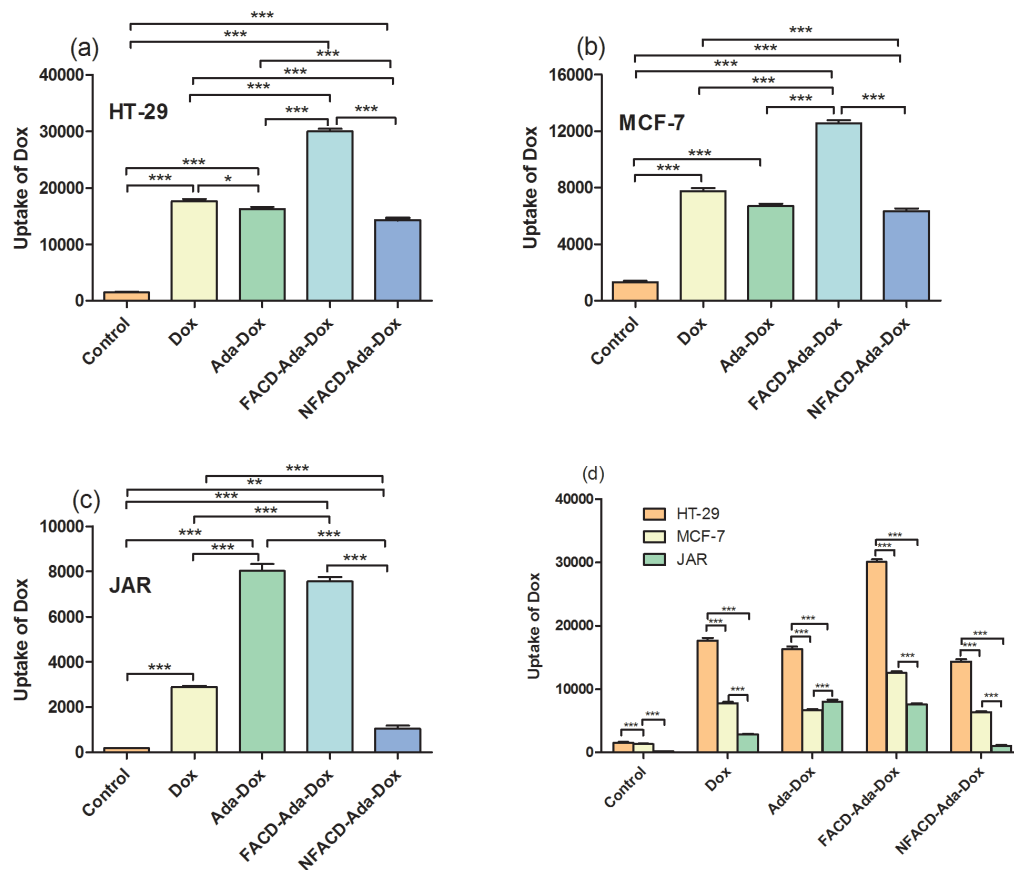


**Figure 10.** The Dox-related fluorescence intensity in HT-29, MCF-7 and JAR cells treated with Dox, Ada-Dox, FACD-Ada-Dox or NFACD-Ada-Dox. The drug at 5.0  $\mu\text{M}$  was added into the 35-mm petri dishes containing  $2 \times 10^5$  cells in 3.0 ml culture medium. The cells were incubated for 2 hr to allow uptake of the drugs. The harvested cells were stained with 20  $\mu\text{l}$  DAPI at 1.0  $\mu\text{M}$  for flow cytometric analysis. Cells incubated with DMEM alone were used as the control. \*\* $P<0.01$ ; \*\*\* $P<0.001$ .  
doi:10.1371/journal.pone.0062289.g010

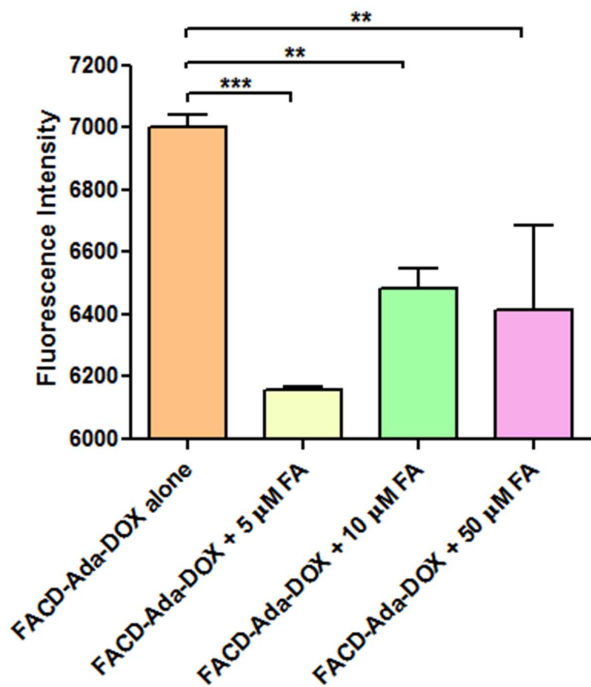


**Figure 11. The uptake of FACD-Ada-DOX at 2  $\mu$ M in JAR cells in the presence of folic acid at 5, 10 or 50  $\mu$ M.** The results are represented as means  $\pm$  SD from triplicate determinations. \*\* $P < 0.01$ ; \*\*\* $P < 0.001$ .

doi:10.1371/journal.pone.0062289.g011

FLOR1) that is an energy-dependent, high-affinity, low-capacity folate-binding protein anchored in the plasma membrane through a glycosylphosphatidylinositol moiety and translocate folates unidirectionally into cells via an endocytotic process; and c) a ubiquitously expressed proton-coupled folate transporter (PCFT/SLC46A1) [27]. Unlike FR $\alpha$ /FLOR1, both RFC and PCFT are membrane-spanning receptors that facilitate bidirectional transport of reduced folate across the plasma and endosomal membranes. Members of the FR family include FR $\alpha$ /FLOR1, FR $\beta$ /FLOR2, FR $\gamma$ /FLOR3, and FR $\delta$ /FLOR4, which can bind FA and reduced folates, and transport them into cells. FR $\alpha$ /FLOR1 and FR $\beta$ /FLOR2 are both GPI-anchored proteins with two *N*-glycosylation sites, with a high affinity for FA ( $K_d = \sim 1$  nM). In normal tissue, FR $\alpha$ /FLOR1 is mainly expressed on the apical surface of a subset of polarized epithelial cells whereas its aberrant expression has been prominently correlated with malignancies of epithelial origin. FR/FR $\alpha$ /FOLR1 is highly over-expressed (40–90%) on primary and metastatic human cancers of the ovary, lung, breast, colon, endometrium, kidney, and brain, but has only limited distribution in healthy tissues [28–30]. This exclusivity has led to the exploitation of FA as an important ligand for specific targeting by diagnostic or therapeutic agents. Even after conjugation to nano-drug complexes, FA acts as a high-affinity ligand ( $K_d > 10^{-10}$  M), enhancing tumor uptake with little involvement of non-tumor tissue compared to conventional chemotherapy. FA derivatization allows the selective delivery of cytotoxic or diagnostic agents to pathologic tissue in the presence of normal cells, and FR can readily and actively internalize bound FA and FA-conjugated compounds via receptor-mediated endocytosis [28,29]. It is hypothesized that FA conjugation to anticancer drugs will improve drug selectivity, thereby avoiding the collateral damage that accompanies their uptake by healthy cells.

For the first time, we have successfully synthesized and purified novel water-soluble, FA-conjugated  $\beta$ -CD-based targeting drug

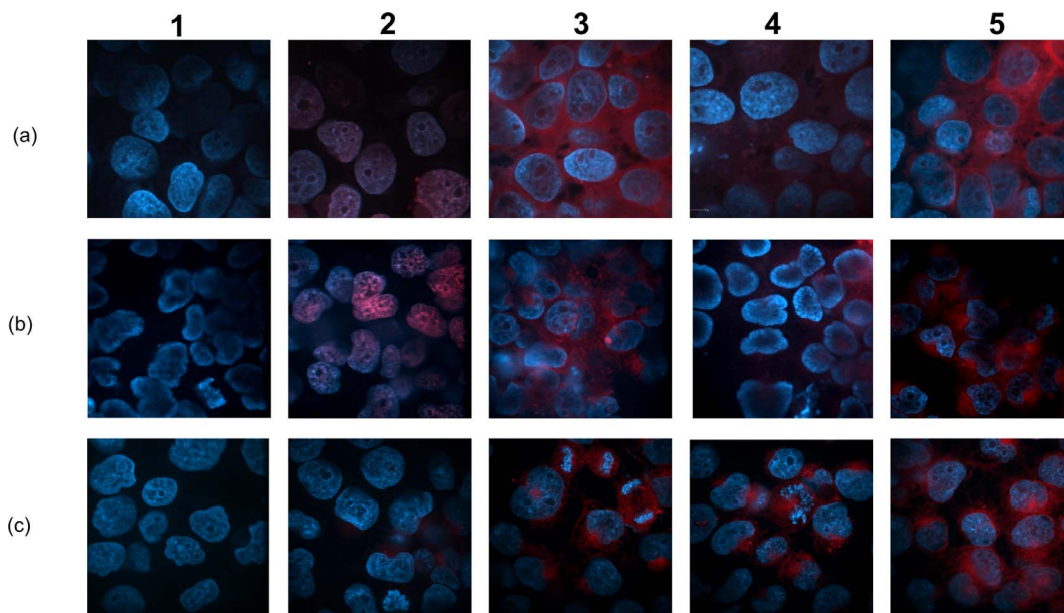


**Figure 12. The intracellular localization of the drugs in JEG-3 and JAR cells and time-dependent drug uptake in JAR cells as exhibited by confocal laser scanning microscopy.** Plots a1–5: JEG-3 cells; b1–5 and c1–5: JAR cells. For rows a & b, 1: Control; 2: Dox; 3: Ada-Dox; 4: NFACD-Ada-Dox; and 5: FACD-Ada-Dox. Plots c1–5 shows the time-dependent drug uptake with FACD-Ada-Dox for 0, 45, 75, 90 and 105 min. Images are merged from 2 channels 405<sub>Exc</sub>, 445<sub>Em</sub> for DAPI and 488<sub>Exc</sub>, 615<sub>Em</sub> for drugs. Both channels utilized the 445 (W60) and 615 (W70) filter sets, respectively. All images are 630 times of magnification with the same contrast adjustment applied across all samples. Images are representative of two independent experiments.

doi:10.1371/journal.pone.0062289.g012



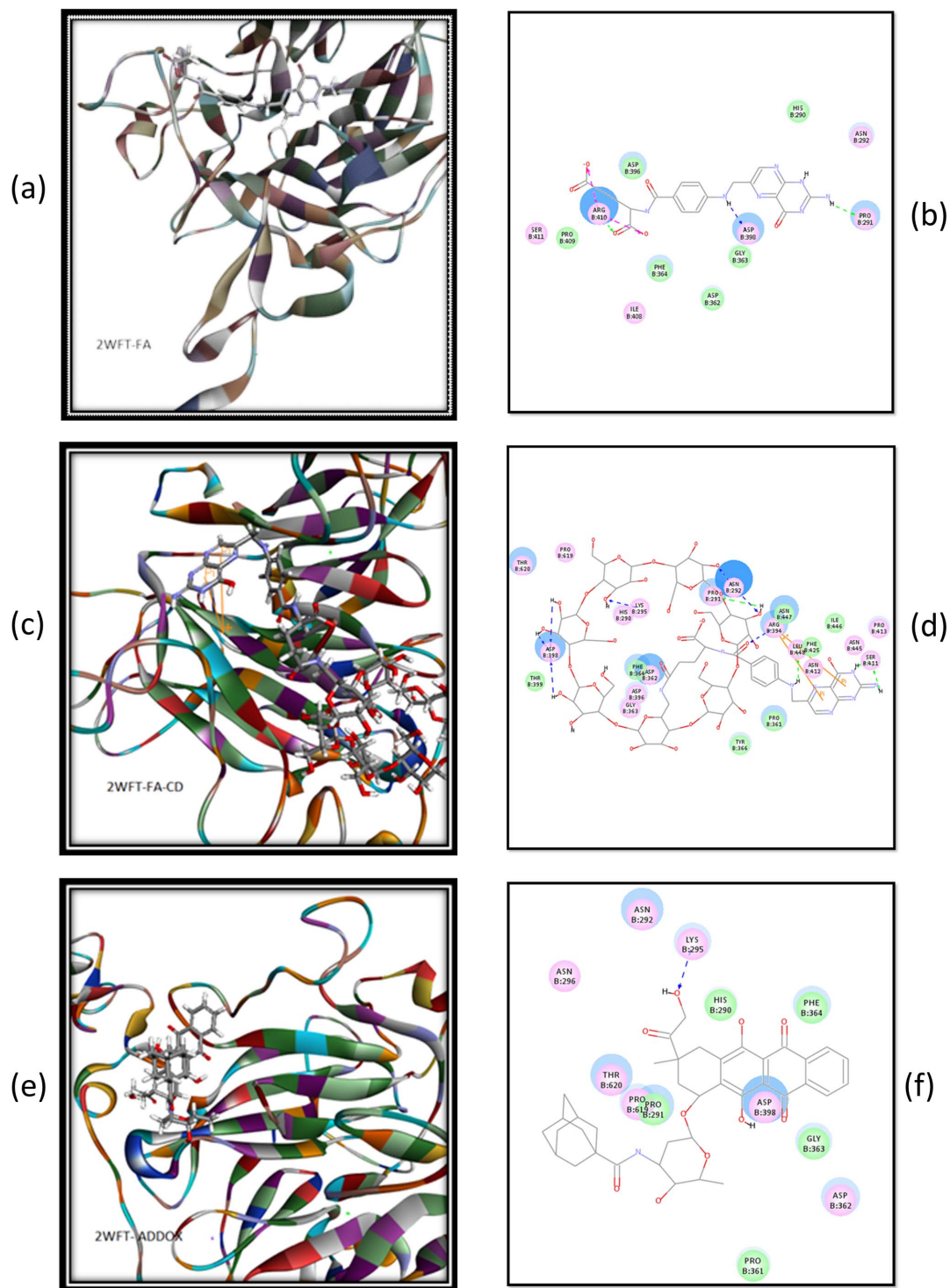


**Figure 13. The binding modes of FA (a & b), FA-CD (c & d) and Ada-Dox (e & f) with human HIPP containing an FR $\alpha$  domain.** The structure of human HIPP containing a human FR $\alpha$  domain (PDB ID: 2WFT) was used in the docking study using the Discovery Studio 3.1 program. doi:10.1371/journal.pone.0062289.g013

supramolecules with ada-Dox as the therapeutic cargo. The structures of the newly synthesized FACDs have been confirmed by spectral methods including NMR, MALDI-TOF-MS, FTIR, CD, and HPLC. So far as we know, this is the first successful preparation of water-soluble, FA-conjugated CD isomers and dimers.

The solvent-suppressed  $^1\text{H-NMR}$  spectrum of  $\gamma$ -FACD clearly showed signals at 6.5 ppm and 7.3 ppm corresponding to aromatic protons of the FA residue and 8.3 ppm for the proton in pteridine structure in FA molecule of FACD carrier (**Figure 3**).  $\alpha$ -FACD produced similar signals but was shifted downfield by 0.15–0.2 ppm relative to  $\gamma$ -FACD; the appearance of the multiple

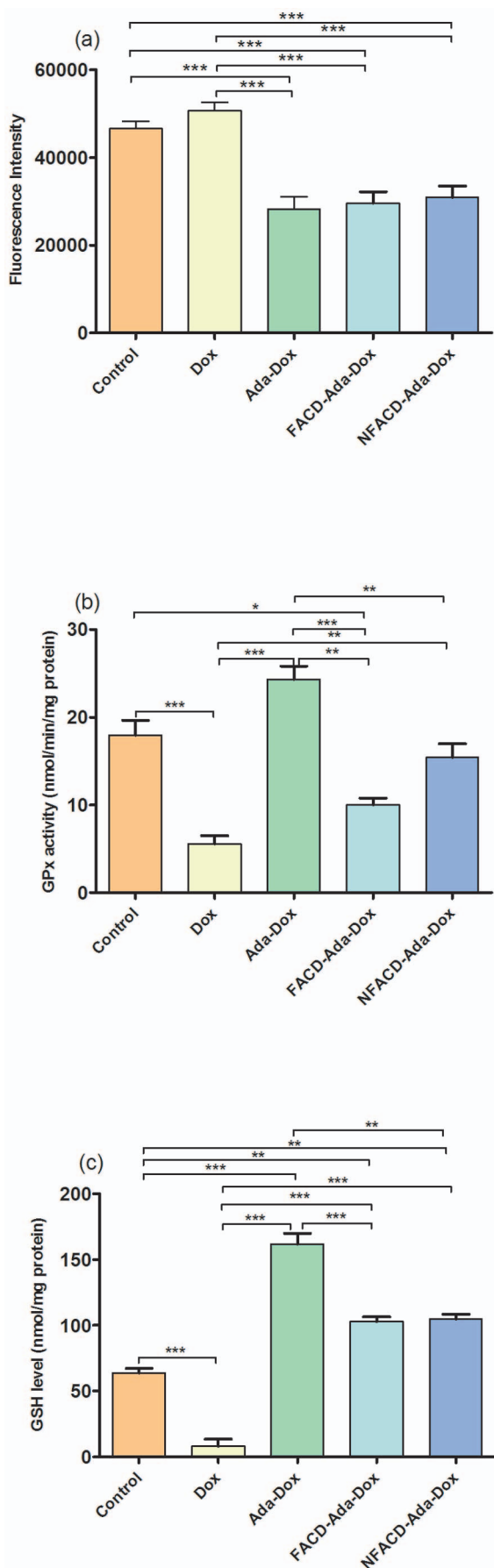


**Figure 14. Determination of intracellular ROS, GPx and GSH levels in mouse heart H9C2(2-1) cells.** Plot a shows the level of intracellular ROS in H9C2(2-1) cells treated with Dox, Ada-Dox or FACD-Ada-Dox at 2.0  $\mu$ M for 18hr at 37°C in the culture media. Cells were treated with CM-H<sub>2</sub>DCFDA. Plot b displays the activity of GPx in H9C2(2-1) cells in the presence of Dox, Ada-Dox or FACD-Ada-Dox at 2.0  $\mu$ M. Plot c shows the GSH concentrations (expressed as nmol/mg protein) in H9C2(2-1) cells in the presence of Dox, Ada-Dox or FACD-Ada-Dox at 2.0  $\mu$ M. Values are the mean  $\pm$  SD of three different homogenates of cells analyzed in triplicate. \* $P$ <0.05; \*\* $P$ <0.01; and \*\*\* $P$ <0.001. doi:10.1371/journal.pone.0062289.g014

proton resonance at 2.0 to 5.0 ppm were assigned to the protons in the CD framework for  $\alpha/\gamma$  substituted isomers as well as FACD.

Cyclodextrins are cyclic oligomers of  $\alpha$ -D-glucose bonded through  $\alpha$ -(1, 4) linkages formed during bacterial digestion of cellulose. The shape of a CD molecule is similar to a truncated cone with a hydrophilic outer surface and a lipophilic central cavity. CDs are widely used as functional macro cyclic host molecules in supramolecular chemistry due to their low cost, water solubility, and biocompatible properties, along with their substantial ability to entrap drug molecules within their internal cavity [31,32].  $\beta$ -CD has the capability to encapsulate up to seven water molecules, and the main driving force of complex formation is the release of enthalpy-rich water molecules from the cavity. Water molecules are displaced by more hydrophobic guest molecules present in the solution to attain an apolar association and decrease of CD ring strain, which results in a lower, more stable energy state in which substitution affects the electron density and the conjugation system. The binding of guest molecules within the host CD is not fixed or permanent but rather is in dynamic equilibrium. The signal from the protons of water is suppressed in our experiment and we found that the CD bucket in the FACDs could entrap the solvent mixture (1-propanol/ethyl acetate/water/ammonium hydroxide) as well as trace amount of free folate to form oily, light yellow complex with similar polarity. While it competed with other solvents when dissolved, the complexation could interfere with the NMR spectrum to some extent. This by-product could be removed through repeated recrystallization.

The formation of guest-host inclusion complexes between Ada-Dox and CDs has proven to be an excellent model system for studying the nature of noncovalent bonding forces in aqueous solution [33]. The interaction of Ada-Dox with CDs resulted in  $\beta$ -CD with an inner-cavity diameter of  $\sim 7.0$  Å. The adamantyl group of Ada-Dox also had a diameter of  $\sim 7$  Å, and it has been confirmed that the strongest binding occurred between adamantane and  $\beta$ -CD, consistent with the near-perfect match between the cavity and guest diameter. The CD spectra also support the host-guest interaction between FACD and the adamantane group of Ada-Dox (Figure 4). Our findings indicate that Ada-Dox interacts with FACD and results in conformational changes at the CD cavity binding site followed by chiral microenvironment changes for the whole drug complex supramolecule.

Besides targeting function, the FACD-Ada-Dox complex is intended to control the release of drug. Folic acid-attached CDs preserve the ability to form non-covalent complexes with the guest drug and in so doing altering their physicochemical properties. The retarded and sustained drug release profile was observed for FACD-Ada-Dox. At the same drug load, the cumulative release of the prodrug in water after 1.5 hr approached 50% compared to <20% in the prodrug, which is desired to improve efficacy and minimize toxicity.

**Table 3.** Effects of the drug complexes on ROS levels, GPx activity and intracellular GSH cofnents in mouse H9C2(2-1) cardiomyocytes and 3T3 fibroblast cells.

Cell type	FACD-Ada-Dox vs Dox			Ada-Dox vs Dox			NFACD-Ada-Dox vs Dox			FACD-Ada-Dox vs NFACD-Ada-Dox		
	ROS (↓)	GPx (↑)	GSH (↑)	ROS (↓)	GPx (↑)	GSH (↓)	ROS (↓)	GPx (↑)	GSH (↑)	ROS (↓)	GPx (↓)	GSH (↓)
<b>H9C2(2-1)</b>												
Change (%)	41.6±3.7	80.0±8.2	1,953.0±20.1	5.1±2.2	58.8 ±2.0	17.4±12.1	44.4±20.8	337.0±77.9	307.0±88.9	39.1 ±3.8	177.1±26.5	1,955.4±69.8
P value	0.0003	0.0209	0.0001	0.55	0.0010	0.0026	0.0003	0.0004	<0.0001	0.0004	0.0056	0.0001
<b>3T3</b>												
Change (%)	17.5±7.63	26.4±5.3	43.4±0.5	2.5±6.5	26.3±0.7	41.8±18.4	19.5±1.8	0.02±5.1	1.2±20.7	-	29.1±5.3	38.3±1.7
P value	0.0048	0.0191	0.0107	0.4933	0.0287	0.0085	0.0071	0.9982	0.9035	-	0.0059	0.995

↑ : increase; ↓ : decrease.  
doi:10.1371/journal.pone.0062289.t003

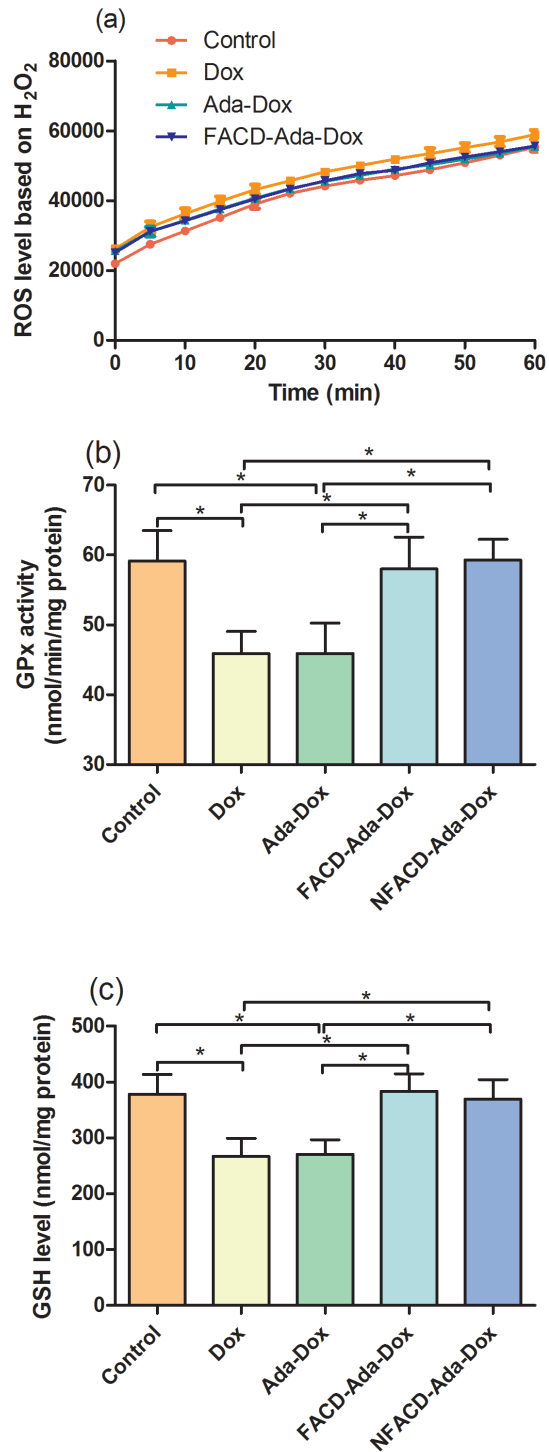


**Figure 15. Determination of intracellular ROS, GPx and GSH levels in mouse 3T3 cells.** Plot a shows the level of intracellular ROS in 3T3 cells treated with Dox, Ada-Dox or FACD-Ada-Dox at 5.0 μM over 60 min at 37°C in the culture media. Cells were treated with CM-H<sub>2</sub>DCFDA. Plot b displays the activity of GPx in 3T3 cells in the presence of Dox, Ada-Dox or FACD-Ada-Dox at 5.0 μM. Plot c shows the GSH concentrations (expressed as nmol/mg protein) in 3T3 cells in the presence of Dox, Ada-Dox or FACD-Ada-Dox at 5.0 μM. Values are the mean ± SD of three different homogenates of cells analyzed in triplicate. \*P<0.05; \*\*P<0.01; and \*\*\*P<0.001.  
doi:10.1371/journal.pone.0062289.g015

The targeted drug FACD-Ada-Dox exhibits significantly enhanced cellular uptake compared with the non-targeted drugs by FR(+) JAR cells. The tumor targeting of FACD-Ada-Dox facilitates faster and increased cellular internalization than NFACD-Ada-Dox. The ligand binding strategy allows preferential internalization of FACD-Ada-Dox into FR(+) cancer cells. FACD-Ada-Dox is taken up at a rate of eight times faster than NFACD-Ada-Dox, while for the HT-29 and MCF-7 cells on which FR is poorly expressed, the binding affinity is comparable among Dox, Ada-Dox, FACD-Ada-Dox, and NFACD-Ada-Dox, except that targeting results in slightly higher drug uptake than non-targeted drugs. The uptake of the targeted drug molecule in JAR cells was significantly inhibited by folate at 5–50  $\mu\text{M}$ . This offers further evidence that the targeted nanoparticles are internalized through FR-mediated pathway. Consistently, the cell killing effects of FACD-Ada-Dox are significantly higher than NFACD-Ada-Dox in FR(+) cells.

It is expected that alleviating cardiotoxicity and enhancing the anticancer efficacy will be achieved when Dox is administered in a slow-release targeting drug complex allowing specific accumulation in tumor cells and reducing the free radicals thought to cause cardiotoxicity. The classical strategies to improve the efficacy and reduce organ toxicity of Dox include: a) enhancing Dox uptake by tumor cells via proper targeting approach and nanotechnology; b) Dox-based prodrugs that can readily activated within tumor cells via liposomal encapsulation or conjugation with antibodies, peptides, or synthetic polymers; c) diminishing Dox deactivation; d) reducing Dox efflux from tumor cells that is often mediated by active drug transporters such as MDR1; e) blocking the antioxidant defense of tumor cells; and f) modulating signaling pathways and cell cycles to sensitize tumor cells to Dox therapy [34]. Each of these means has certain advantages and limitations and sometimes a combination of these strategies may be required to maximize tumor cell killing and minimize organ toxicity [35].

The clinical usage of Dox is limited by cumulative, dose-related, progressive myocardial damage that may lead to congestive heart failure in cancer patients [15]. The cardiotoxicity induced by Dox appears to be a multi-factorial process caused primarily by oxidative stress-induced free radicals involving both Dox and its toxic metabolites such as doxorubicinol [13,15]. The mechanism for the therapeutic effect of Dox is thought to be different from that of its cardiotoxicity. The slow-releasing targeted drug complex is expected to elicit less deleterious effects on normal cells. The results showed that ROS accumulation inside cells after FACD-Ada-Dox and Ada-Dox treatment was less than for free Dox in both mouse H9C2(2-1) cardiomyocytes and fibroblast 3T3 cells. Furthermore, the activity of GPx and GSH content were significantly increased in H9C2(2-1) cells treated with FACD-Ada-Dox compared to cells treated with free Dox. This suggests that the higher GSH levels seen with FACD-Ada-Dox could be sufficient to remarkably decrease ROS levels, thereby maintaining the function and increasing survival for normal cardiomyocytes under chemotherapy.

The protective effect of FACD-Ada-Dox is more apparent than the prodrug Ada-Dox in both H9C2(2-1) cardiomyocytes and fibroblast 3T3 cells. This suggests that targeting FR in FR(+) cardiomyocytes is not the main determinant for Dox-induced cardiotoxicity. A lower ROS production and higher increase in GPx activity and GSH content in cells treated with FACD-Ada-Dox than Ada-Dox can be ascribed to a lesser release of free Dox from the FR-targeted complex than the prodrug Ada-Dox, resulting in less uptake of cardiotoxic Dox. A more significant protection of FACD-Ada-Dox and Ada-Dox in H9C2(2-1) cardiomyocytes than fibroblasts is likely due to differential

expression of FR protein and binding affinity to FRs. In addition, the distinct expression and activity levels of RFC and PCFT in different types of cells that participate in FA transport across the membrane may also contribute to the differential protection observed in this study. Drug treatment time is another important factor that can affect the Dox-induced ROS production and the protective effect of FACD-Ada-Dox and Ada-Dox. A longer drug exposure may facilitate the conversion of Dox to its cardiotoxic metabolites such as 7-deoxy-doxorubicinone and doxorubicinol, thereby enhancing the signaling transduction for the production of ROS and reactive nitrogen species.

In this study, we synthesized the Ada-Dox conjugate rather than Dox as the cargos. Adamantine has very strong host-guest interaction by molecular recognition and high binding affinity with the cyclodextrin cavity since the geometry of the adamantane fits well with the inner cavity, and in this way the drug will be entrapped tightly by CD molecules and thus reducing drug release. Another reason is that Ada-Dox preserve strong fluorescence and we could readily trace the drug inside cells.

Based on the data from our MTT, cellular uptake and binding and cardiomyocyte protection assays, the prodrug Ada-Dox has showed totally different behaviors compared to free Dox. It is less toxic to the cancer cells than Dox *in vitro* and can protect the cardiomyocytes from Dox-induced injuries. These findings suggest that design of prodrugs for Dox represents an alternative way to ameliorate the organ toxicity and enhance the anticancer efficacy of Dox. A number of Dox-based prodrugs have been synthesized and reported [36–38], but their efficacy and safety profiles must be validated in cancer patients.

Since the crystal structure of human FR members is not resolved so far, we used the structure of HHIP containing a FR $\alpha$  domain to examine whether conjugation of  $\beta$ -CD could affect the FA-FR binding. The results showed that both FA and FACD could be readily docked into the possible binding site of HHIP and Ada-Dox could form weak binding with HHIP. Because FACD-Ada-Dox is a supramolecule with noncovalent binding, we have difficulties in generating this larger molecule and docking into HHIP using the CDocker module in Discovery Studio 3.1. Our docking results suggest that FA, FACD and FACD-Ada-Dox could bind the FRs on the surface of cancer cells and thus facilitate endocytosis.

In summary, we have reported the successful synthesis and purification of novel water soluble, folic acid-conjugated  $\beta$ -cyclodextrin-based targeting drug supramolecules with adamantane-doxorubicin as the therapeutic cargo. The structures have been rigorously characterized by HR-MALDI-TOF-MS, 1D/2D NMR, FTIR, HPLC, and circular dichroism. The targeted drug complex possesses high drug association and sustained drug release properties with good biocompatibility and physiological stability. Cellular uptake and FR binding competitive experiments demonstrated an efficient and preferentially targeted delivery of Dox into FR-positive carcinomatous cells. Moreover, the decrease in ROS levels and increase in GPx activity and GSH content in cardiomyocytes exposed to the targeted Dox complex indicate the cardiotoxicity by doxorubicin could be ameliorated by the selective targeting of FR. The novel folic acid-conjugated  $\beta$ -CD based drug complex reported here might be promising as an anti-tumor treatment. *In vivo* animal studies are undertaking at our laboratory.

## Supporting Information

**Figure S1** The  $^1\text{H-NMR}$  spectrum of Ts-CD (400 MHz, D<sub>2</sub>O). (TIF)

**Figure S2 The ESI-MS spectrum of Ts-CD.**

(TIF)

**Figure S3 The ESI spectrum of  $\beta$ -CD (a) and  $\text{NH}_2$ -CD (b).**

(TIF)

**Figure S4 LC-MS spectra of Ada-DOX (a & b).**

(TIF)

**Figure S5 The  $^1\text{H-NMR}$  (a, 800 MHz,  $\text{D}_2\text{O}$ ) and  $^{13}\text{C-NMR}$  (b, 201 MHz,  $\text{D}_2\text{O}$ ) spectra of  $\gamma$ -FACD.**

(TIF)

**Figure S6 The g-COSY spectra of  $\gamma$ -FACD (a, 600 MHz,  $\text{D}_2\text{O}$ , and when zoomed within 6–8 ppm, b).**

(TIF)

**Figure S7 The  $^1\text{H-NMR}$  (a, 600 MHz,  $\text{D}_2\text{O}$ ) and  $^{13}\text{C-NMR}$  (b, 201 MHz,  $\text{D}_2\text{O}$ ) spectra of  $\alpha$ -FACD.**

(TIF)

**Figure S8 The g-COSY spectra of  $\alpha$ -FACD (a, 600 MHz,  $\text{D}_2\text{O}$ ; when zoomed within 6–8 ppm, b).**

(TIF)

**Figure S9 The  $^1\text{H-NMR}$  spectrum of FA-diCD (600 MHz,  $\text{D}_2\text{O}$ ).**

(TIF)

**Figure S10 The original HR-MALDI-TOF spectrum of FA-diCD.**

(TIF)

**Figure S11 The original HR-MALDI-TOF spectrum of  $\gamma$ -FACD.**

(TIF)

**Figure S12 The original HR-MALDI-TOF spectrum of  $\alpha$ -FACD.**

(TIF)

**Figure S13 The FTIR spectra of  $\beta$ -CD (a), N3-CD (b),  $\text{NH}_2$ -CD (c), FA (d), and  $\gamma$ -FACD (e).**

(TIF)

**Figure S14** (a) The HPLC-ELSD chromatogram of  $\beta$ -CD (black),  $\text{NH}_2$ -CD (blue) and  $\gamma$ -FACD (Magenta); (b) HPLC-UV chromatogram of  $\beta$ -CD (Magenta),  $\text{NH}_2$ -CD (blue) and  $\gamma$ -FACD (black); and (c) HPLC-DAD chromatograms of Ada-Dox (35 min), Dox (9 min) and FACD-Ada-Dox (1.5 min).

(TIF)

**Acknowledgments**

The authors wish to thank Drs. Szekeres Karoly and Amanda Garces at the Lisa Muma Weitz Advanced Microscopy Core Laboratory, Dr. Robert W. Buzzeo at the Department of Cell Biology, Microbiology and Molecular Biology, College of Arts and Sciences, and Dr. Emirov Yusuf at the Nanotechnology Research & Education Center, University of South Florida, Tampa, Florida, USA. We also thank Drs. Edwin Rivera and David Badge at the NMR Facility at the University of South Florida, and appreciate Dr. Laurent Calcul for the performance of HPLC-ELSD and Dr. Kumar Mohanraja for the technical assistance of Mass Spectrometer at the Department of Chemistry, University of South Florida, Tampa, Florida, USA.

**Author Contributions**

Conceived and designed the experiments: JJY ZWZ YZ PG CZL JRK TY SSM WL WD JCW QL XZ JT LJ JL MQW XL SFZ. Performed the experiments: JJY SS SPS ZXW. Analyzed the data: JJY XZ JT CZL MQW SFZ. Wrote the paper: JJY SS SPS. Edited the paper: PG CZL JRK TY SSM JT XZ SFZ.

**References**

- Thun MJ, DeLancey JO, Center MM, Jemal A, Ward EM (2010) The global burden of cancer: priorities for prevention. *Carcinogenesis* 31: 100–110.
- Ferlay J, Shin HR, Bray F, Forman D, Mathers C, et al. (2010) Estimates of worldwide burden of cancer in 2008: GLOBOCAN 2008. *Int J Cancer* 127: 2893–2917.
- Gatenby RA (2009) A change of strategy in the war on cancer. *Nature* 459: 508–509.
- Chabner BA, Roberts TG Jr (2005) Timeline: Chemotherapy and the war on cancer. *Nat Rev Cancer* 5: 65–72.
- Cotter TG (2009) Apoptosis and cancer: the genesis of a research field. *Nat Rev Cancer* 9: 501–507.
- Yague E, Raguz S (2005) Drug resistance in cancer. *Br J Cancer* 93: 973–976.
- Petros RA, DeSimone JM (2010) Strategies in the design of nanoparticles for therapeutic applications. *Nat Rev Drug Discov* 9: 615–627.
- Muro S (2012) Challenges in design and characterization of ligand-targeted drug delivery systems. *J Control Release* 164: 125–137.
- Lammers T, Kiessling F, Hennink WE, Storm G (2012) Drug targeting to tumors: principles, pitfalls and (pre-) clinical progress. *J Control Release* 161: 175–187.
- Wang AZ, Langer R, Farokhzad OC (2012) Nanoparticle delivery of cancer drugs. *Annu Rev Med* 63: 185–198.
- Kizek R, Adam V, Hrabeta J, Eckschlagler T, Smutny S, et al. (2012) Anthracyclines and ellipticines as DNA-damaging anticancer drugs: recent advances. *Pharmacol Ther* 133: 26–39.
- Octavia Y, Tocchetti CG, Gabrielson KL, Janssens S, Crijns HJ, et al. (2012) Doxorubicin-induced cardiomyopathy: from molecular mechanisms to therapeutic strategies. *J Mol Cell Cardiol* 52: 1213–1225.
- Minotti G, Menna P, Salvatorelli E, Cairo G, Gianni L (2004) Anthracyclines: molecular advances and pharmacologic developments in antitumor activity and cardiotoxicity. *Pharmacol Rev* 56: 185–229.
- Dickey JS, Rao VA (2012) Current and proposed biomarkers of anthracycline cardiotoxicity in cancer: emerging opportunities in oxidative damage and autophagy. *Curr Mol Med* 12: 763–771.
- Menna P, Paz OG, Chello M, Covino E, Salvatorelli E, et al. (2012) Anthracycline cardiotoxicity. *Expert Opin Drug Saf* 11 Suppl 1: S21–36.
- Salas C, Perez-Vera P, Frias S (2011) Genetic abnormalities in leukemia secondary to treatment in patients with Hodgkin's disease. *Rev Invest Clin* 63: 53–63.
- Mo SL, Liu WF, Li CG, Zhou ZW, Luo HB, et al. (2012) Pharmacophore, QSAR, and binding mode studies of substrates of human cytochrome P450 2D6 (CYP2D6) using molecular docking and virtual mutations and an application to chinese herbal medicine screening. *Curr Pharm Biotechnol* 13: 1640–1704.
- Mo SL, Liu WF, Chen Y, Luo HB, Sun LB, et al. (2012) Ligand- and protein-based modeling studies of the inhibitors of human cytochrome P450 2D6 and a virtual screening for potential inhibitors from the Chinese herbal medicine, *Scutellaria baicalensis* (Huangqin, Baikal Skullcap). *Comb Chem High Throughput Screen* 15: 36–80.
- Bishop B, Aricescu AR, Harlos K, O'Callaghan CA, Jones EY, et al. (2009) Structural insights into hedgehog ligand sequestration by the human hedgehog-interacting protein HHIP. *Nat Struct Mol Biol* 16: 698–703.
- Roy PP, Roy K (2010) Pharmacophore mapping, molecular docking and QSAR studies of structurally diverse compounds as CYP2B6 inhibitors. *Mol Simul* 36: 887–905.
- Wu G, Robertson DH, Brooks CL 3rd, Vieth M (2003) Detailed analysis of grid-based molecular docking: A case study of CDocker-A CHARMM-based MD docking algorithm. *J Comput Chem* 24: 1549–1562.
- Eruslanov E, Kusmartsev S (2010) Identification of ROS using oxidized DCFDA and flow-cytometry. *Methods Mol Biol* 594: 57–72.
- Wang H, Joseph JA (1999) Quantifying cellular oxidative stress by dichloro-fluorescein assay using microplate reader. *Free Radic Biol Med* 27: 612–616.
- Beutler E, Duron O, Kelly BM (1963) Improved method for the determination of blood glutathione. *J Lab Clin Med* 61: 882–888.
- Petter RC, Salek JS, Sikorski CT, Kumaravel G, Lin FT (1990) Cooperative binding by aggregated mono-6-(alkylamino)- $\beta$ -cyclodextrins. *J Am Chem Soc* 112: 3860–3868.
- Crider KS, Yang TP, Berry RJ, Bailey LB (2012) Folate and DNA methylation: a review of molecular mechanisms and the evidence for folate's role. *Adv Nutr* 3: 21–38.
- Sabharanjak S, Mayor S (2004) Folate receptor endocytosis and trafficking. *Adv Drug Deliv Rev* 56: 1099–1109.
- Hilgenbrink AR, Low PS (2005) Folate receptor-mediated drug targeting: from therapeutics to diagnostics. *J Pharm Sci* 94: 2135–2146.
- Zhao X, Li H, Lee RJ (2008) Targeted drug delivery via folate receptors. *Expert Opin Drug Deliv* 5: 309–319.

30. Weitman SD, Lark RH, Coney LR, Fort DW, Frasca V, et al. (1992) Distribution of the folate receptor GP38 in normal and malignant cell lines and tissues. *Cancer Res* 52: 3396–3401.
31. Davis ME, Brewster ME (2004) Cyclodextrin-based pharmaceuticals: past, present and future. *Nat Rev Drug Discov* 3: 1023–1035.
32. Chen G, Jiang M (2011) Cyclodextrin-based inclusion complexation bridging supramolecular chemistry and macromolecular self-assembly. *Chem Soc Rev* 40: 2254–2266.
33. Granadero D, Bordello J, Perez-Alvite MJ, Novo M, Al-Soufi W (2010) Host-guest complexation studied by fluorescence correlation spectroscopy: adamantane-cyclodextrin inclusion. *Int J Mol Sci* 11: 173–188.
34. Hanusova V, Bousova I, Skalova L (2011) Possibilities to increase the effectiveness of doxorubicin in cancer cells killing. *Drug Metab Rev* 43: 540–557.
35. Kratz F, Warnecke A (2012) Finding the optimal balance: Challenges of improving conventional cancer chemotherapy using suitable combinations with nano-sized drug delivery systems. *J Control Release* 164: 221–235.
36. Fan J, Fang G, Zeng F, Wang X, Wu S (2012) Water-dispersible fullerene aggregates as a targeted anticancer prodrug with both chemo- and photodynamic therapeutic actions. *Small*.
37. Hochdorffer K, Abu Ajaj K, Schafer-Obodozie C, Kratz F (2012) Development of novel bisphosphonate prodrugs of doxorubicin for targeting bone metastases that are cleaved pH dependently or by cathepsin B: synthesis, cleavage properties, and binding properties to hydroxyapatite as well as bone matrix. *J Med Chem* 55: 7502–7515.
38. Legigan T, Clarhaut J, Renoux B, Tranoy-Opalinski I, Monvoisin A, et al. (2012) Synthesis and antitumor efficacy of a  $\beta$ -glucuronidase-responsive albumin-binding prodrug of doxorubicin. *J Med Chem* 55: 4516–4520.